

This is a repository copy of *Development of calcium sulfoaluminate-belite cements for the encapsulation of radioactive waste*.

White Rose Research Online URL for this paper: https://eprints.whiterose.ac.uk/id/eprint/232886/

Version: Accepted Version

Article:

Nelson, S. orcid.org/0009-0003-8888-8541, Cockburn, S., Tuck, O. et al. (6 more authors) (2026) Development of calcium sulfoaluminate-belite cements for the encapsulation of radioactive waste. Cement and Concrete Composites, 165. 106355. ISSN: 0958-9465

https://doi.org/10.1016/j.cemconcomp.2025.106355

© 2025 The Authors. Except as otherwise noted, this author-accepted version of a journal article published in Cement and Concrete Composites is made available via the University of Sheffield Research Publications and Copyright Policy under the terms of the Creative Commons Attribution 4.0 International License (CC-BY 4.0), which permits unrestricted use, distribution and reproduction in any medium, provided the original work is properly cited. To view a copy of this licence, visit http://creativecommons.org/licenses/by/4.0/

Reuse

This article is distributed under the terms of the Creative Commons Attribution (CC BY) licence. This licence allows you to distribute, remix, tweak, and build upon the work, even commercially, as long as you credit the authors for the original work. More information and the full terms of the licence here: https://creativecommons.org/licenses/

Takedown

If you consider content in White Rose Research Online to be in breach of UK law, please notify us by emailing eprints@whiterose.ac.uk including the URL of the record and the reason for the withdrawal request.



Development of calcium sulfoaluminate-belite cements for the

encapsulation of radioactive waste

- 3 Shaun Nelson ¹, Sally Cockburn ¹, Olivia Tuck ¹, Martin Hayes ¹, Gavin Cann ¹,
- 4 Cameron Halliwell ², Daniel Geddes ², Brant Walkley ², Stephen Farris ³
- ¹ United Kingdom National Nuclear Laboratory (UKNNL), Workington, Cumbria, CA14 3YQ, UK
- 6 ² School of Chemical, Materials, and Biological Engineering, University of Sheffield, S1 3JD, UK
- ³ Sellafield Ltd, Seascale, Cumbria, CA20 1PG, UK

1. Highlights

1

2

8

9

10

11

12

13

14

15

16

17

18

19

20

21

22

2324

25

26

27

2829

3031

32

3334

35

- CSA is a potentially attractive alternative encapsulant, particularly due to the ability for ettringite to tie up large amounts of water and immobilise ionic species.
- Mixes were conducted using both laboratory scale and encapsulation plant equipment.
- Paper highlights the properties of mixes, including their hydrate assemblage, and the feasibility of their adoption in an encapsulation process, even when undiluted by waste.
- Despite the high hydration temperatures, hydrate assemblage remains substantially unchanged suggesting that ionic species retention may persist even under these exceptional operating conditions, providing a bounding case.

2. Abstract

To demonstrate and evaluate the potential of calcium sulfoaluminate-belite (CSA) cements for the enhanced encapsulation of future higher activity waste treatment processes, a commercially available clinker was trialled on a 3 L scale, before being scaled up to 500 L scale, using a typical In-Drum mixing (IDM) methodology and equipment employed for the encapsulation of radioactive slurry wastes in the UK. The formulation envelope varied the gypsum addition, water to solid ratio, and mixing shear regime. Mixes were conducted neat, with no addition of waste material, additives, supplementary cementitious materials, or fillers. Conducting IDM standard mixes allowed for the trial of formulations in absence of waste loading during operations, subjecting products to hydration exotherm temperatures based upon the scale of the products cast in excess of normal operations, where waste incorporation would be expected to dilute the peak hydration exotherm obtained. This scenario allows for the behaviour of the main CSA strength giving phase ettringite to be evaluated, establishing a bounding case. Following a curing duration of 28 and 90 d, the phase assemblage between products subjected to different curing exotherms were indistinguishable, despite being subjected to a range of different temperature profiles and the structure of the 500 L products being compromised. Processing properties were consistent between mixing scales, with physical properties producing desirable results when not impacted by the high exotherm temperatures experienced by 500 L products.

Keywords: Calcium sulfoaluminate; belite; sulfate; ettringite; nuclear waste;

immobilisation; encapsulation

3. Introduction

Calcium sulfoaluminate (CSA) cement is under consideration by the UK nuclear industry as a potentially promising alternative encapsulant for the processing and treatment of radioactive waste [1]. CSA has been shown to have lower associated CO₂ emissions and is being developed as an addition or alternative to Portland cements (PC), such as CEM I, principally for applications requiring rapid strength development and high dimensional stability [2], [3], [4]. It may offer advantages over currently employed PC-based encapsulants, with properties such as enhanced chemical resistance and the ability to incorporate typically retarding materials, an early age pore solution pH below 12 thereby reducing the initial rate of amphoteric metal corrosion, and high-water retention allowing for fluid mixes to penetrate complex wasteforms without the generation of residual bleed liquor [1], [5], [6], [7]. Historically, the UK nuclear industry has used CEM I grouts with a majority ground granulated blast furnace slag (GGBS) or pulverised fly ash (PFA) supplementary cementitious material (SCM) component [8], [9]. GGBS has remained in use at Sellafield Intermediate Level Waste (ILW) encapsulation plants, with the GGBS to CEM I ratio used having reached as high as 9:1 [1], [10].

These SCMs both enhance the performance of the wasteform by reducing long-term permeability, altering redox chemistry of the matrix in the case of GGBS, and reducing the peak temperature reached during early-stage hydration as their rate of reaction is much slower compared to PC [11], [12]. Both these SCMs are by-products of heavy industries (coal fired power and steel manufacturing respectively) which are in decline in the UK, and securing a supply of standardised material capable of delivering the required enhanced performance characteristics has therefore become a greater challenge in recent years [10], [13], [14]. The development of alternative cement systems, driven by their unique performance characteristics and the need to reduce the contribution of cement manufacturing towards global anthropogenic CO₂ emissions, as well as a potential improvement in the longer-term security of the supply of powder materials, has led the UK nuclear industry to explore the potential use of such systems [15].

CSA-belite cements contain a majority of ye'elimite ($C_4A_3\hat{S}$) with a smaller quantity of belite (C_2S). When combined with a source of calcium sulfate, such as gypsum, the main product of ye'elimite is ettringite (the archetype of the "AFt" – tri – phase family of hydrous calcium

sulfoaluminates) with aluminium hydroxide (gibbsite or amorphous) (Eq. 1) ¹. If a sufficient

72 quantity of calcium sulfate is not available, then calcium monosulfoaluminate (monosulfate)

73 will form, a representative of the AFm (*mono*) phase family (Eq. 2) [1], [5], [6], [7], [16], [17].

74

75 (Eq. 1)
$$C_4A_3\hat{S} + 2C\hat{S}H_2 + 34H \rightarrow C_3A \cdot 3C\hat{S} \cdot 32H + 2AH_3$$

76 (Eq. 2)
$$C_4A_3\hat{S} + 18H \rightarrow C_3A \cdot C\hat{S} \cdot 12H + 2AH_3$$

77

78 Belite typically hydrates slowly, over a matter of months, forming either calcium silicate

79 hydrate (C-S-H) (Eq. 3), or the silica-substituted AFm phase strätlingite (Eq. 4) [3], [18].

80

81 (Eq. 3)
$$C_2S + 2H \rightarrow C-S-H + CH$$

82 (Eq. 4)
$$C_2S + AH_3 + 5H \rightarrow C_2ASH_8$$

83

8687

84 Ettringite is attributed with early strength development, with belite hydration products

85 contributing towards longer term development. Ettringite crystals form in a hexagonal

prismatic columnar morphology and have been shown to host a number of ions within the

columnar and channel sections of the AFt crystal structure, as well as through substitution of

88 the calcium (e.g. by Ba²⁺), aluminium (e.g. by Cr³⁺), hydroxide, and sulfate sites (e.g. by IO₃-

and AsO_4^{3-}) [17], [19], [20], [21], [22]. The belite hydration product C-S-H has also been shown

90 to host a number of ionic species [23]. As a result, the CSA system is a potentially attractive

91 matrix for the immobilisation of waste species, which may prove advantageous as part of an

92 engineered barrier system (EBS), as well as the potential for chemically binding a high

proportion of mix water content, thereby producing highly fluid mixes whilst reducing the

propensity for the system to produce bleed [1].

9596

98

101

93

94

The stability of ettringite is a relationship between temperature and the availability of water,

97 wherein dehydration and topotactic decomposition, with the reduction of 30 - 32 to 9 - 13

moles H₂O per mole of Al₂O₃, forms meta-ettringite [24]. This relationship is demonstrated by

299 Zhou et al. (2001) [25] and Baquerizo et al. (2016) [26] as a hysteresis loop, wherein the

reformation of ettringite occurs if the temperature is low enough alongside the availability of

water being high enough [25], [26]. Meta-ettringite retains the ettringite needle crystal

structure in all 3 dimensions, and the same Ca/Al/S ratios, with the distance between

ettringite cation columns reduced producing an amorphous phase [24], [27], [28]. It is as yet

unclear if the presence of meta-ettringite is detrimental to CSA in terms of strength,

¹ Chemical reaction equations in this paper are presented using cement chemistry abbreviated notation, where C represents CaO, A is Al₂O₃, S is SiO₂, H is H₂O, and Ŝ is SO₃.

dimensional stability, or the retention of radionuclides, with some studies demonstrating the enhanced anion retention properties of meta-ettringite over ettringite [29], [30], [31].

Temperatures in excess of 100 °C can result in the decomposition of ettringite to monosulfate along with the precipitation of calcium sulfate [25], [32]. Monosulfate can also react to form ettringite, given the availability of calcium sulfate and water, known in PC chemistry as delayed ettringite formation [33], [34], [35].

Currently employed encapsulant grouts based on blended PC systems are designed to conform to an acceptance criteria with dependence upon its application. A broad, guideline example that may be considered suitable is provided below:

• The cumulative heat of hydration output ideally should not exceed 180 kJ/kg of blended cementitious powders after 24 h hydration at 35 °C. Grout temperature should be kept below 100 °C to mitigate potential impacts upon product integrity. However, if heat outputs above these values are shown not to detrimentally affect subsequent wasteform product properties, this does not preclude use of a matrix as an encapsulant for ILW treatment.

• Fluidity ², after mixing and additional hold-up time of 150 mins, should ideally exceed a Colflow measurement of 500 mm to allow adequate penetration of wastes via flood grouting operations without applying vibration to minimise product voidage (see Sections 4.3.1 and 4.4 for mixing and Colflow methodology). When immobilising liquid or slurry wastes, upon mixing with cementitious materials, the grout should be fluid enough to produce a homogeneous product.

• An initial set should not be achieved in less than 2 h from end of mixing for 500 L products produced via an In-Drum mixing (IDM) methodology, with a final set being achieved within 48 h. This is determined using a Vicat test (Section 4.6).

• The grout should not have a bleed layer > 2 vol.% on 100 mL sealed samples produced from small-scale (\sim 3 L mixes) after 24 h from the end of additional mixing at 150 mins.

• Compressive strength development must be sufficient to only retain the structural stability of the product, as structural loads will be taken up by the product container and supporting structural furniture. As low as 4 MPa at 7 d has historically been taken as an acceptable guideline for strength development [36], [37].

² In rheological terms, fluidity is defined as the ability for a material (grout) to deform or flow under applied stress (gravity during Colflow). High fluidity indicates a low resistance to deformation or flow.

• Dimensional stability must be such that long-term physical stability is maintained to ensure cracking is minimised, radionuclide immobilisation is not compromised, and hence essentially monolithic products are produced over prolonged periods of storage. Historic acceptable limits for grouted ILW products are typically based on +1000 microstrain (+0.1 %) expansion to -3000 microstrain (-0.3 %) shrinkage ³. This is only viewed as acceptable once dimensional changes have stabilised.

• The chemistry of the cements system should allow for maximum waste loading, by not affecting these conditions because of insufficient chemical compatibility.

A currently employed acceptance criteria may not necessarily represent the ideal usage of the CSA-belite system but will act as a guidance when comparing against current systems. This is also true for many standards when using alternative cement systems in other applications [38].

This work is aimed at furthering the understanding of the behaviour of the CSA-belite mixes when scaled up for use in a full size commercial encapsulation plant. In particular, the assessment of the thermal stability of ettringite following peak exotherm in an undiluted full scale mix scenario. This is trialled as a bounding case, where if the phase assemblage remains stable under these conditions, then it is anticipated to remain stable at the expected lower operational temperatures. In a more typical scenario, encapsulated waste would likely act to dilute the exotherm of a product and as a result reduce the peak product temperature. Therefore, ettringite would be expected to remain stable with the incorporation of waste, assuming no significant exothermic chemical interactions occur. Similarly, before SCMs can be included in the mix design, it is important to understand how a grout might behave in a full scale undiluted scenario.

This is achieved by evaluating and comparing a series of mixes conducted on both a 3 L and 500 L scale to determine potential CSA-belite formulations for ILW encapsulation, utilising commercially available CSA-belite clinker and gypsum. Further investigations can then be undertaken as to the durability and interactions of CSA-belite wasteforms as part of an EBS environment, as per the UK's chosen final disposal program employing a deep geological facility (GDF).

³ Dimension stability is a strain measurement based on the change in length over a unit length, thus 1 microstrain = 1×10^{-6} m/m or 1×10^{-3} mm/m, so 1000 microstrain = 1 mm/m.

Work has been published previously covering the phase assemblage of CSA-belite mixes conducted at the 3 L scale, principally in Nelson et al. (2023) [17], which shall be referenced for context and comparison [17], [39].

173174175

176

171

172

4. Experimental

- 177 **4.1.** Materials
- 178 A commercially available CSA-belite clinker was selected for use in both 3 L and 500 L mixes,
- accompanied by commercially sourced calcium sulfate in the form of gypsum. As a result of
- the time between both trials being conducted and the batch production of powders, the CSA
- and gypsum used have been termed either CSA-3 or CSA-500 (and gypsum-3 or gypsum-
- 182 500) to distinguish between batches used for each set of trials. X-ray diffraction (XRD) data
- 183 was provided by the suppliers for each batch of powder using Rietveld analysis. The CSA
- clinker contains a relatively high ve'elimite and low belite content, with the CSA-3 containing
- 60.8 wt.% $C_4A_3\hat{S}$, 14.8 wt.% β- C_2S , and 2.7 wt.% $C\hat{S}$, and CSA-500 containing 59.1 wt.% $C_4A_3\hat{S}$,
- 186 7.7 wt.% C₂S, and 2.5 wt.% CŜ. The gypsum-3 and gypsum-500 consist of 100 wt.% and 99
- 187 wt.% CŜH₂ respectively.

188

- Powders were tested for fineness by air permeability, particle size distribution (PSD) using
- laser diffraction on a Malvern Mastersizer 3000 utilising an aero dispersion unit with a
- refractive index (RI) of 1.68 for CSA and 1.53 for gypsum, loss on ignition (LoI) at 950 °C, and
- 192 particle density by pyknometer using a liquid displacement technique as specified in BS EN
- 193 1097-7:2008 [40]. Chemistry by X-ray fluorescence (XRF) using a fused bead technique, and
- 194 chloride and sulfate analysis as specified in EN 196-2:2013, were also provided by the suppliers
- of each batch of powder.

- Table 1: Powder properties for those employed in both 3 L and 500 L mixes, denoted as, e.g., CSA-3 and CSA-
- 198 500.

Powder	Fineness (m²/kg)	LOI (wt.%)	Particl	e Size (µn		bution	Particle Density	Average Specific Surface Area (µm ⁻¹) 5			
	(III / Ng)	(Dv10	D _v 50	D _v 90	Span ⁶	(g/cm ³)	Surface Area (µm -)			
CSA-3	528	0.87	2.5	11.5	39.0	3.2	2.87	0.52			
CSA-500	556	0.65	2.1	13.4	51.4	2.8	2.82	0.45			
Gypsum-3	385	20.94 ⁷	4.6	37.2	134.0	3.5	2.36	0.16			
Gypsum-500	372	20.71 ⁷	4.7	33.6	104.0	2.3	2.32	0.18			

Table 2: XRF powder characterisation for those employed in both 3 L and 500 L mixes, denoted as, e.g., CSA-3 and CSA-500.

Powder	X-Ray Fluorescence Analysis (wt.%) ⁷											
Towder	Al ₂ O ₃	SiO_2	Na ₂ O	K ₂ O	TiO ₂	Fe ₂ O ₃	CaO	MgO	SO_3	Cl -		
CSA-3	29.49	9.35	0.97	0.55	0.42	1.37	39.81	4.17	7.26	0.13		
CSA-500	32.85	7.21	1.03	0.54	0.47	1.27	38.33	4.69	11.55	0.11		
Gypsum-3	< 0.02	0.16	< 0.02	0.01	< 0.03	< 0.01	32.71	< 0.04	46.20	-		
Gypsum-500	0.11	0.50	0.01	0.04	0.01	0.04	32.18	0.08	45.41	-		

4.2. Mix Formulations and Curing

3 L mixes were conducted as part of a series of mixes developing a potential formulation envelope of CSA with different levels of calcium sulfate. The gypsum addition was either 15, 25, or 35 wt.% of the total pre-blended solids in the mix design. The water to solids mass ratio (w/s), calculated on the basis of total solids (clinker + calcium sulfate), was set to either 0.5, 0.6 or 0.7 [17]. A low or high mixing shear rate method was also used (Section 4.3.1).

Guided by the 3 L study, two 500 L scale mixes were conducted using CSA-500 clinker blended with either 20 or 35 wt.% gypsum and a w/s mass ratio of 0.65 or 0.60 respectively. These mixes fell within the recommended formulation envelope from the 3 L studies from a processing and product property perspective, whilst covering a 'higher' exotherm mix with lower gypsum content and higher water content, and a corresponding 'lower' exotherm mix with higher gypsum and lower water content.

 $^{^4}$ Dv10, Dv50, and Dv90 represent the equivalent particle diameter at which 10, 50 and 90 % of the sample volume falls below.

 $^{^{5}}$ Average specific surface area = 3 / (Dv50 / 2) [41].

⁶ Span shows the width of the size distribution, giving an indication of how far the 10% and 90% size fractions are apart, normalised by the midpoint = (Dv90-Dv10) / Dv50.

⁷ Data provided by the manufacturer/supplier.

Table 3: Identifying names used for the two 500 L scales mixes.

500 L Scale Mix Reference	Gypsum Addition (wt.%)	Water to Solids Ratio (w/s)
5G20	20	0.65
5G35	35	0.60

4.3. Mixing Methodologies

4.3.1. Mixes at the 3 L Scale

Before mixing, CSA clinker and calcium sulfate powders were pre-blended. Powder and water temperatures used were in the range of 16 ± 1 °C. Deionised water was added to the Hobart N50 mixer shortly before mixing began at 62 rpm, wherein the pre-blended powder was added over a period of 5 mins. After a further 5 mins, high shear mixes were switched to a Silverson L5 overhead mixer for 10 mins and mixed at 4500 rpm, whilst low shear mixes remained on the Hobart N50 at 62 rpm for the total 20 mins.

At this point, the time is denoted as t=0. Additional hold-up mixing was then carried out at 62 rpm for a maximum of 150 mins (t=150). Colflow fluidity assessments (Section 4.4) were made every 30 mins, with mixes concluded and samples cast if grout fluidity measurements were ≤ 500 mm or deemed likely to fall to this value within the next 30 mins based on the fluidity trends observed with time.

4.3.2. Mixes at the 500 L Scale

Before a mix, CSA clinker and gypsum were weighed out into a hopper to the nearest 0.5 kg as per the accuracy of the load cell. A 500 L product drum was also prepared with a thermocouple supporting frame (Section 4.7). Both the hopper and drum were then pre-heated to 20 ± 1 °C in a cure cell before installation into the mixing rig. The required amount of domestic mains water at between 14 – 15 °C was then weighed and added. The mixer is a bespoke 500 L capacity rig equipped with a Rushton turbine.

The mixer was started with a paddle speed of 460 rpm with powders being discharged over a 12 min period. Paddle speed was reduced to a minimum of 297 rpm to avoid splashing after 10 min of powder addition. After powder addition was complete, mixing continued at 297 rpm for a further 10 min (22 min total), after which the paddle speed was reduced to \sim 180 rpm for hold-up. At this point, the time is denoted as t=0. At t=0, each mix was assessed for fluidity and analytical products were taken. Once all smaller products had been cast (8 min after t=0), the remaining grout was discharged over a 15 min period into the pre-prepared 500 L product

drum. This was then covered with a plastic sheet to reduce evaporative losses and cured in a cure cell at 20 ± 1 °C.

4.4. Fluidity

The fluidity of a mix was measured by Colcrete flow channel based on the method defined in BS EN 13395-2:2002 [42]. At the time of measurement (Section 4.3), 1 quart (1.14 L) of grout is released from a tundish positioned above a wetted, level channel (Figure 1). Once released, the grout is allowed to flow under gravity and the subsequent distance reached, after allowing to rest for 60 s, is recorded against the scale upon the channel. If the grout fluidity measurement achieved is \leq 500 mm, then any hold-up period will end, and all products are cast. The maximum length of flow that the channel can record is 1020 mm.

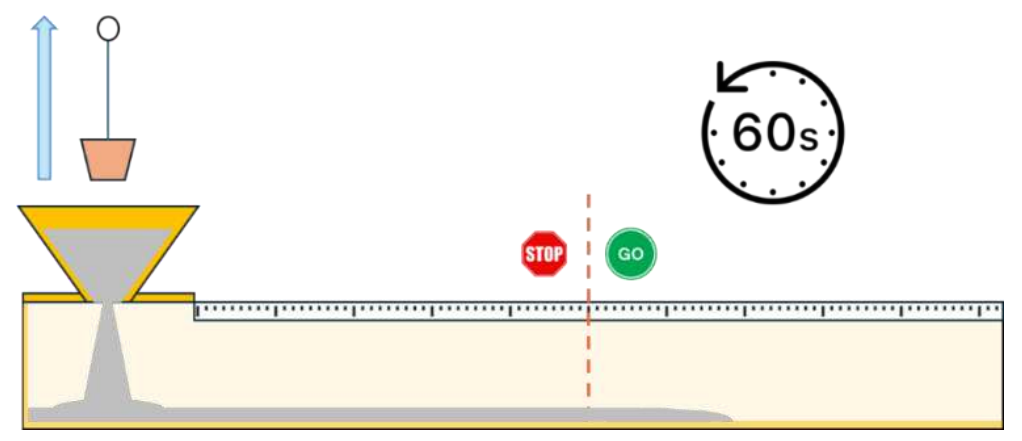


Figure 1: Illustration of the Colflow fluidity measurement technique, showing the 500 mm fluidity mark which will result in the termination of any mix hold-up period.

4.5. Bleed

Bleed measurements were conducted using grout collected at t=0 for 3 L and 500 L mixes, and t=150 for 3 L mixes (or when the Colflow fluidity measurements dropped to \leq 500 mm). Samples were cast into a 100 mL measuring cylinder which were sealed and cured at 20 \pm 1 °C for 24 h, with bleed expressed as vol·vol%-1.

4.6. Setting Behaviour

Initial and final set was determined by manual Vicat apparatus on 160 mL samples based on the method described in BS EN 196-3:2005 [43]. These were taken at t=150 (or when the Colflow fluidity measurements dropped to \leq 500 mm) for 3 L mixes, and t=0 for 500 L mixes. Samples were cured at 20 \pm 1 °C, with samples sealed with fitted lids between measurements and the set times recorded referring back to t=0.

4.7. Heat of Hydration

Cumulative heat flow and normalised heat flow were measured on samples taken from 3 L scale mixes at t=0 using a TAMAir isothermal conduction calorimeter (ICC). A 1 g sample was used, sealed inside a glass vial preheated to 35 °C, with the ICC set to a base temperature of 35 °C representing pessimistic Sellafield Ltd (SL) encapsulation plant treatment cell conditions. The heat of hydration was calculated based on the total mass of solids (CSA clinker + gypsum) present in the grout sample, therefore normalising to account for the water content.

Prior to conducting the 500 L mixes, two wooden frames were constructed each supporting twelve type K thermocouples across six locations. One frame was positioned in each 500 L drum to allow the exotherm of the products to be monitored. The thermocouples were located at the bottom, middle and top of the product at both the centre and outer (\sim 100 mm from the side) positions as shown in Figure 2. With a product height of \sim 1 m for a 500 L product, the bottom, middle and top thermocouples were positioned 100, 450, and 800 mm from the bottom of the drum respectively. Each drum was covered with a plastic sheet to prevent evaporative losses and cured at 20 \pm 1 °C.

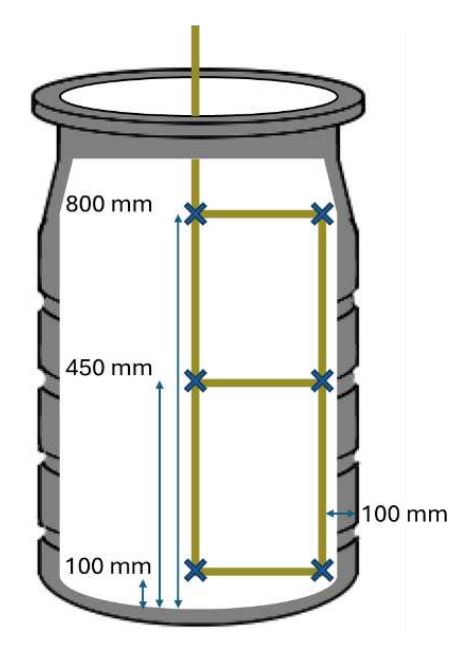


Figure 2: Schematic showing six thermocouple positions (marked 'x') attached to a supporting frame within each 500 L drum.

4.8. Sample Production and Preparation

4.8.1. Samples Produced from 3 L Mixes

Each 3 L scale mix produced four $286 \times 26 \times 26$ mm rectangular prisms for dimensional stability testing, twelve 40 mm cubes for product strength analysis, two 100 mL measuring cylinders for bleed measurement at t=0 and t=150 (end of mixing), and one 160 mL polypot sample for set measurement. Several samples were also cast in sealed centrifuge tubes (15 ml) for microstructural analysis. Dimensional stability prisms were wrapped in polythene to

prevent samples drying out, with only measurement end studs being exposed [44]. All samples were cured in a controlled 20 ± 1 °C high humidity (> 90 %RH) walk in chamber and placed in sealed polythene bags to reduce evaporative losses once demoulded, before being processed as per Section 4.8.3.

4.8.2. Samples Produced from 500 L Mixes

From each 500 L scale mix, four 200 \times 100 mm cylinders were cast separately from the main product for compressive strength testing, and one 160 mL polypot sample for set measurement. After 7 d curing and demoulding, these four smaller cast cylinders were cut down to produce four 100 \times 100 mm samples, from each smaller cast cylinder, using a powered masonry saw. This was in order to produce samples for testing in duplicate which matched the dimensions of the majority of cored samples taken from the large scale product.

The 500 L product from mix 5G20 was demoulded after 7 d curing. Due to the manner in which the product broke up during demoulding, the interior surface of the product was exposed without sectioning. Two 100 \times 100 mm cored cylinders were taken from the top of 5G20, with four smaller cores of 40 \times 40 mm taken from the middle and bottom of the sample in order to work around the fracture planes. The 500 L product from mix 5G35 was demoulded after 6 d curing to assess whether it was possible to section this product. This product was deemed to have sufficient integrity for sectioning and, as a result, was cut in half from top to bottom to expose the internal surface.

Four 100 \times 100 mm cores were taken from 5G35, again due to stresses present in the product preventing the intended six cores from being obtained. Coring locations from both products are shown in Figure 3, with coring achieved using a wet coring method. All samples, either cast or cored, were cured in a 20 \pm 1 °C controlled environment until required for testing, and either covered or sealed in containers or polythene bags to reduce evaporative losses once demoulded, before being processed as per Section 4.8.3.

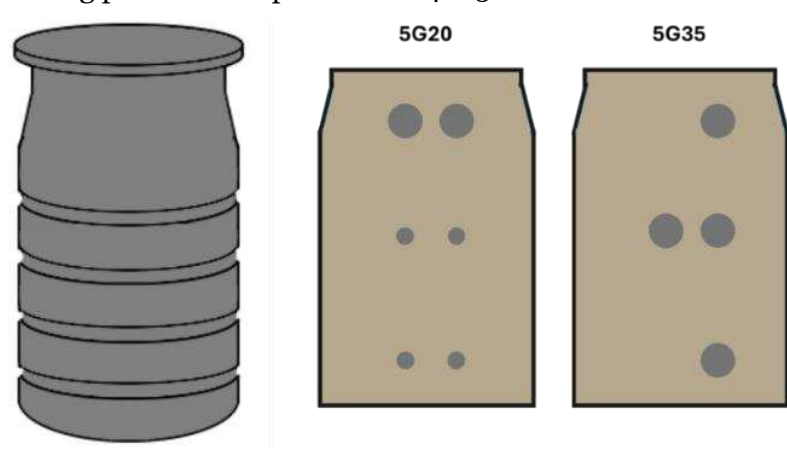


Figure 3: Locations of successful 500 L product cores taken. Larger circles are depicting 100 \times 100 mm cylinder, with smaller circles representing the smaller 40 \times 40 mm cylinder cores taken.

335336337

338339

340

341

342

343

344

345

334

4.8.3. Microstructural Analysis Preparation

For microstructural analysis of the 3 L scale mixes, remains from compressive strength cubes tested at 7, 28, and 90 d were ground and sieved to between 0.5-2 mm particle size, before being subjected to an arresting hydration solvent exchange method as proposed by Lothenbach & Scrivener [45]. 15 mL samples were also cast in centrifuge tubes and cured for either 7, 28, or 90 d. These were then cut into \sim 15 mm long cylinders and also subjected to the same arresting hydration solvent exchange method. For this, samples were submerged in isopropanol, which was routinely changed over a period of hours, to facilitate the removal of free water from the system. These were then dried to a constant weight in a desiccator at 25 °C.

346347348

349

350

351

352

353

354

355

From 500 L mixes, samples for 28 and 90 d microstructural analysis were sourced from the smaller cast cylinders, or cores taken following compressive strength testing, from the maximum and minimum temperature regions measured during the product exotherm. In the absence of core samples available at 28 d from the 500 L 5G20 product, both 28 and 90 d samples were sourced directly from the product. Samples were either ground and sieved, or retained as \sim 15 mm long pieces, and subjected to the same arresting hydration solvent exchange method as previously described [45]. All samples, when not being processed or analysed, were stored in either a nitrogen filled sealed bag, or a vacuum desiccator, and at a room temperature of \sim 20 °C.

356357358

- 4.9. Scanning Electron Microscopy (SEM) and Energy Dispersive X-ray Spectroscopy (EDS)
- 359 Samples cast within the 15 mL centrifuge tubes of ~ 15 mm in length for SEM were sectioned
- 360 to ~ 5 mm³ before being cold mounted in epoxy resin. These samples were then ground and
- polished in batches of six using a planetary automatic grinding and polishing machine, using
- isopropanol as a rinsing aid. Polishing was carried out up to a 0.25 µm diamond grade. SEM,
- 363 coupled with EDS, was carried out by using a Hitachi TM3030 instrument, with EDS
- 364 conducted using a coupled Quantax 70 detector. An electron accelerating voltage of 15 kV was
- used with a working distance of 8 mm. EDS was conducted at 1000 × magnification, with the
- highlighted elements including Al, Ca, Fe, Mg, Na, Si and S [17].

- 368 4.10. Thermogravimetric Analysis (TGA)
- 369 For analysis by TGA, previously prepared ground samples were further processed to a particle
- size of < 63 μm. TGA was performed using a Perkin Elmer TGA 4000, with data analysed using

- 371 Pyris Manager, wherein $40 \pm 2 \mu g$ of $< 63 \mu m$ powdered sample was heated in an alumina
- 372 crucible from room temperature to 1000 °C, at a heating rate of 10 °C·min⁻¹, under an inert
- 373 nitrogen atmosphere [17].

- 375 4.11. X-ray diffraction (XRD) and Rietveld Analysis
- For analysis by powder XRD, ground samples were further processed to a particle size of < 63
- 377 μm. XRD was performed using a PANalytical X'pert³ and Cu-Kα radiation, at a 2θ range of 5
- 378 70°, a step size of 0.026°, and a time per step of 4 s [17]. Sample holders were backloaded
- with powder sample to reduce the degree of preferred crystal orientation. Rietveld analysis
- was conducted with TOPAS software using the fundamental parameter approach for all
- 381 phases. This was performed using the same setup, model, and working to the same phase
- assemblage as detailed in Nelson et al. (2023) [17] with an average Rwp of 1.83.

383

- 384 4.12. Dimensional Stability
- Dimensional stability testing was carried out at the 3 L scale, with acceptable formulations
- 386 then considered for the 500 L trial. Four $286 \times 26 \times 26$ mm prisms were cast to monitor
- dimensional stability at 2, 7, 28, 56, 70, and 90 d curing. This was achieved in accordance with
- 388 ASTM C490 [44] using a Heidenhain test frame, performed by comparing the length of each
- prism against a stainless steel Invar reference rod to record how the length changed over time
- as the CSA cement hydration reaction proceeds.

391

- 392 4.13. Product Strength
- 393 To monitor and assess the strength development of products cast, ultrasonic pulse velocity
- 394 (UPV) and compressive strength testing was conducted over a 90 d curing period. UPV is an
- indirect, non-destructive measure of the expected strength development of a sample, in which
- 396 the time taken for a longitudinal wave pulse to travel through a specimen is measured. As the
- densification of the specimen microstructure occurs, and therefore its strength increases, the
- 398 time taken for the pulse to travel through the specimen decreases and the UPV increases. UPV
- was conducted using a CNS Farnell Pundit 7.

- 401 Compressive strength testing was carried out using an ELE International ADR Auto V2.0
- 402 2000/250kN range compression machine, with grain density calculated by the equipment
- 403 using Archimedes' principle involving weight in air and water. From each 3 L scale mix, twelve
- 404 40 mm cubes were cast and examined in triplicate using UPV at 2, 7, 28, 56, 70, and 90 d
- 405 curing, and compressive strength testing at 2, 7, 28, and 90 d curing. From each 500 L scale
- 406 mix, smaller cast cylinder samples were tested in pairs at 28 and 90 d curing for UPV and

compressive strength measurement. Cored samples from 5G20 were tested at 51 and 90 d 8 curing due to the challenges experienced during coring with the product exhibiting significant cracking due to thermal stress, whilst cores from 5G35 were tested at 28 and 90 d curing.

4.14. Statistical Analysis

Statistical analysis and associated contour plots were produced in the statistical package R, using linear regression to find relationships between input parameters [46]. Linear regression models take the form shown in Eq. 5, where yi is the independent variable, the xn are the n dependant variables, the βn are the n coefficients to be estimated and εi is the random error. The linear model is then used to make predictions of the effect of changing discrete mix parameters on a particular grout property, such as for example, the cumulative heat of hydration at 24 h curing over the range of percentage sulfate and w/s ratio tested, the resulting model then being shown as a contour plot to illustrate overall trends.

(Eq. 5)
$$yi = \beta 0 + \beta 1xi1 + \dots + \beta nxin + \varepsilon i$$

5. Results at the 3 L Scale

424 5.1. Fluidity

Maintaining adequate grout fluidity is essential for both the successful encapsulation of geometrically complex waste material with minimal voidage and providing the ability to readily mix viscous slurry or sludge wastes to yield a homogeneous product. Fluidity is particularly important when operating without application of vibration, which is desirable due to the complexity of maintaining such equipment in a radioactive environment. A Colflow value of < 500 mm can be deemed at risk of gelation and setting before the process has concluded.

Early-stage fluidity is a function of the available water content, therefore increasing both the water and gypsum content effectively increases the content of available water, with gypsum being a hydrated form of calcium sulfate. Of the formulations evaluated at 3 L, only when at 15 wt.% gypsum content and 0.5 w/s ratio did the predicted fluidity drop < 500 mm during the mixing regime, which occurred at between t=60 and t=150 mins during hold-up time. This is illustrated by the statistical analysis of the 3 L fluidity measurements with time (Figure 4).

 $^{^8}$ The compressive strength of 40 mm cored cylinder samples was calculated based on actual dimensions despite the test taking place in a 40 mm jig. This gave a pessimistic value, ensuring the strengths reported were accurate.

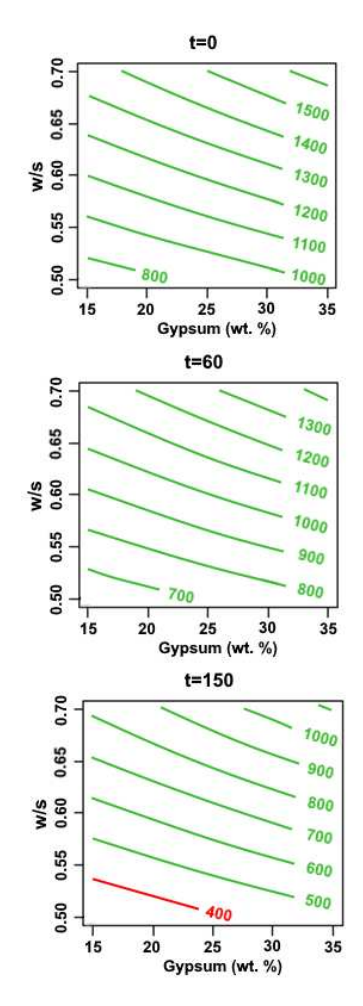


Figure 4: Statistical analysis contour plots generated from the 3 L scale mixes, with contours set at 100 mm Colflow intervals. The red contour represents a value < 500 mm which would result in the mix being halted (outside the desired range).

5.2. Heat of Hydration

 The cumulative heat flow recorded from the 3 L scale mixes all exceed the current technical specification guideline value of 180 J/g for cement powders, based on total powders in the mix (including SCM) used in current encapsulation plant processes (Figure 5). The rapid hydration of CSA generally releases heat at a greater rate than PC, which has been utilised in the past for construction in cold climates, but does not necessarily exceed the total heat generation of PC [47], [48]. However, as discussed in Section 3, currently employed grouts for ILW encapsulation processes contain a majority SCM component with a significantly slower rate of hydration, which will act to dilute the heat output of the system over this time period.

CSA grout in this scenario is being prepared neat, with no SCM or fillers to reduce the heating rate or cumulative heat capacity and therefore represents a maximised heat output scenario. Figure 5 shows a decrease in the cumulative 24 h curing heat flow with increasing gypsum content, but an increase in cumulative heat flow with increasing water content. This is also

shown in the statistical analysis of the formulation envelope (Figure 6). Increasing the availability of water in CSA increases the heat of hydration to a greater extent than that experienced in PC systems [48]. This is likely due to enhancing the hydration mechanism, such as through aiding in the dissolution kinetics of clinker phases and calcium sulfate, as well as the enhanced mobility of ions like aluminium, to produce ettringite at a greater rate (through-solution mechanism) [4], [49]. In contrast, increasing the fraction of gypsum content in the mix will serve to reduce the overall quantity of the highly reactive ye'elimite present, which will dilute the heat output.

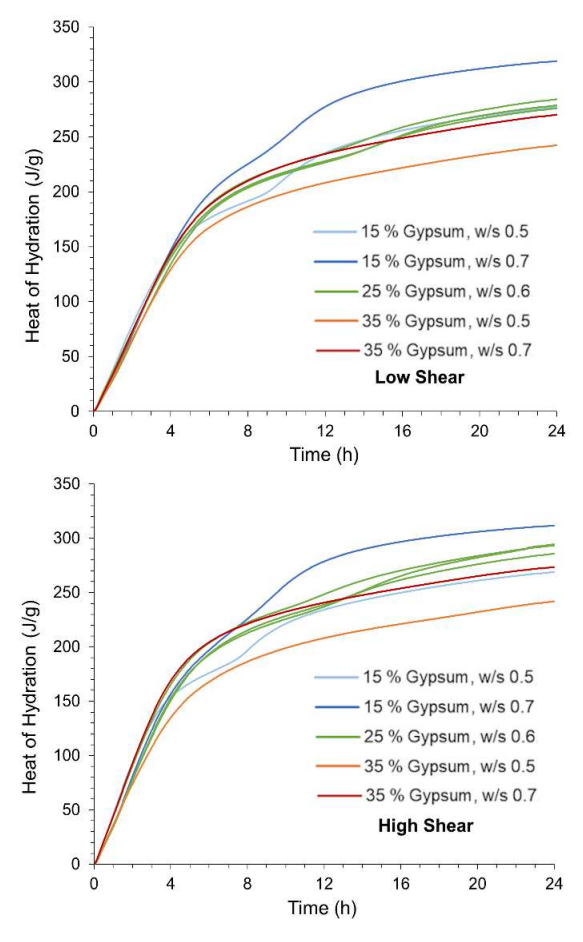


Figure 5: Cumulative heat of hydration with time from 3 L scale mixes, accounting for only the CSA + gypsum content.

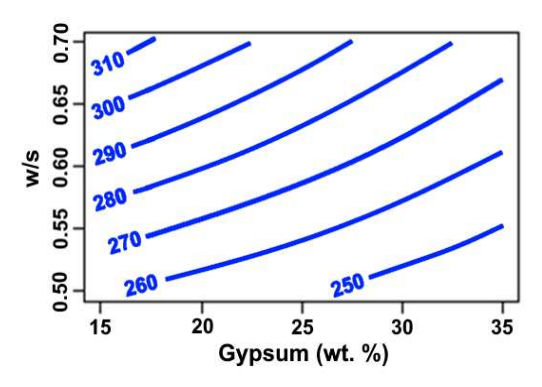


Figure 6: Statistical analysis contour plot generated from the 3 L scale mixes, with contours representing the cumulative heat flow at 24 h in J/g set in intervals of 10 J/g.

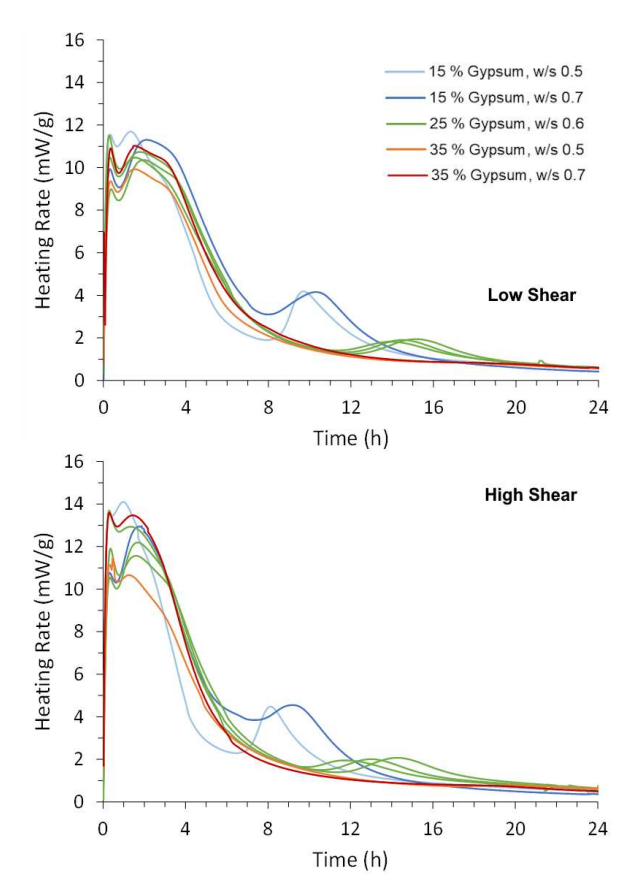


Figure 7: Normalised heat flow with time from 3 L scale mixes.

 The normalised heat flow (Figure 7) shows a relationship between reducing gypsum content and the occurrence of an additional exotherm peak at between 8-16 h. Higher shear mixes have typically increased the heating rate of the early exotherm but not the total heat output during this time period. Notably, the higher shear mixing methodology results in a greater heating rate initially, along with the second main exotherm (8-10 h), if present, occurring sooner. The secondary exotherm is delayed and the rate of heating reduced with increasing gypsum, with it unidentifiable within a 24 h period in mixes containing a 35 wt.% gypsum addition. This profile is similar to that of Winnefeld and Barlag (2010) [50], wherein the peak

encountered at ~ 10 h is attributed to a depletion in the availability of gypsum at this time and an increase in the formation of monosulfate as opposed to ettringite (Eq. 2). Significant increases in levels of monosulfate were not, however, recorded at the first instance of phase assemblage assessment using Rietveld analysis at 7 d [17], [39].

5.3. Setting Behaviour and Bleed

For the purposes of this experimental procedure and to allow a grout enough processing time to be deployed in an IDM process, an initial set requirement of ≥ 2 h has been defined, with a final set achieved ≤ 48 h to allow for the safe transport of waste packages without the risk of compromising product integrity.

In 3 L mixes, both initial and final sets were encountered within 4 h, with the earliest initial set encountered at between 3 and 4 h. Sets were monitored manually, with some products likely achieving set outside of facility operational hours. Setting times captured within the same day are shown in Figure 8, with all mixes conducted achieving a final set < 24 h. The availability of water within the system appears to extend the setting time by a small degree, within the region of ~ 1 h. The availability of water will be impacted by both the w/s ratio, and the quantity of gypsum addition given it is a hydrated form of calcium sulfate. The difference between the high and low shear mixing methods has shown no discernible difference in the setting times. For 24 h cured products, a tolerable bleed of 2 vol.% from small-scale mixes minimises the generation of liquid active waste that requires additional treatment. Bleed occurs when the remaining liquid component exceeds the available volume within the products pore network. All products incorporated all the liquid component and generated no bleed.

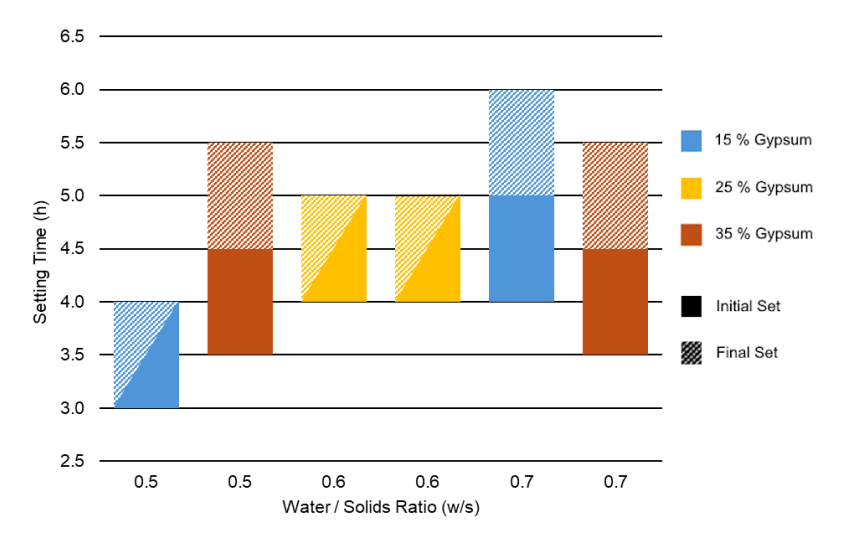


Figure 8: Setting behaviour at the 3 L scale, with recordings taken manually to within an hour for both the initial set (solid fill), final set (diagonal fill), or both if they occurred during the same measurement interval (diagonal fill split).

5.4. Dimensional Stability

Dimensional stability is an important criterion for cementitious waste packages, ensuring that the grouted products maintain their long-term physical stability (upwards of hundreds of years) and that the external container remains uncompromised both structurally and dimensionally, with barriers against the mobilisation of radionuclides remaining intact for a maximised duration in an EBS [36]. Dimensional changes within cemented wasteforms, resulting from the formation of expansive phases, or drying shrinkage through water loss in non-saturated conditions, can lead to cracking of the resultant product if either expansion or shrinkage is excessive.

All recorded measurements remained within \pm 1000 microstrain 9 for the experimental duration 10 , thus remaining within the suggested criteria, with microstrain generally appearing to plateau within this timeframe. Figure 9 shows an increase in microstrain with a gypsum content > 15 %, with slight expansion occurring between 2 and 7 d before a gradual shrinkage rate. The greatest overall shrinkage occurs in 15 wt.% gypsum content mixes, most notably for those with the lowest water. This is not observed in higher gypsum mixes however, where in the highest water content mixes exhibit greater shrinkage. The rate of mixing shear has no impact at upon the dimensional stability of set products.

This overall high dimensional stability suggests that a significant proportion of ettringite precipitation is occurring via a through-solution mechanism as opposed to topotactic. As described by Odler et al. (2000) [4], high aluminium mobility allows for the even precipitation of ettringite within the solution phase, wherein for the topotactic mechanism ettringite forms upon the surface of an anhydrous aluminous phase and exerts expansive stress by applying force to surrounding phases in the direction of its growth. Topotactic formation is encouraged by the concentration of calcium hydroxide (CH, Portlandite), of which only low concentrations have been identified, which would therefore favour the through-solution mechanism [4], [17]. Ettringite growth from points more evenly distributed throughout the high alumina phases or within the solution containing pore network will retain a products dimensional stability to a greater extent.

-

⁹ Dimension stability is a strain measurement based on the change in length over a unit length, thus 1 microstrain = 1×10^{-6} m/m or 1×10^{-3} mm/m, so 1000 microstrain = 1 mm/m.

 $^{^{10}}$ Facility opening days, impacted by Covid-19, limited days that data could be collected. Curing ≥ 90 d was a duration of ~ 110 d.

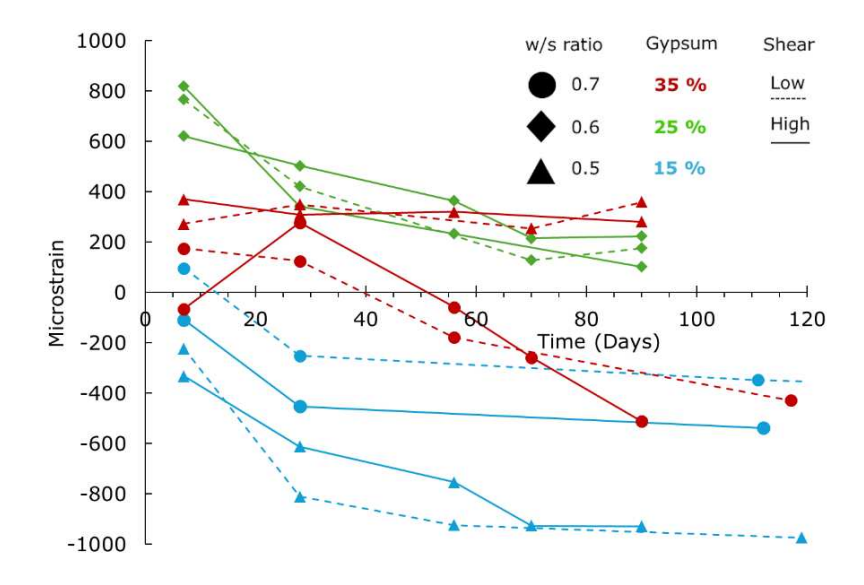


Figure 9: Dimensional stability plot showing microstrain with time, comparing the different mixing variables.

5.5. Product Strength

The strength requirement for a grout product is considerably lower than that of a product for structural applications, with a historically accepted guideline as low as 4 MPa at 7 d and 7 MPa at 90 d for grouted ILW products [36], [37]. The external container contributes the load bearing capacity, with the product inside needing only to resist loss of integrity during handling and storage so as not to increase waste mobility. Nevertheless, strength development is symptomatic of the generation of a stable cementitious phase assemblage, wherein a decrease in strength may be a product of unstable phase development with the development of such undesirable product properties as increasing porosity or internal stresses.

Products produced at the 3 L scale show the characteristic high early strength development of CSA systems with the production of ettringite, far exceeding the required strength given in the suggested criteria (Table 4). This initial 2 d strength is reduced with increasing water content, and to a lesser extent, with increasing gypsum content (Figure 10). An increase in the availability of water allows for a greater presence of free water, which leads to an increase in porosity within a system [51], [52], [53]. The increasing presence of gypsum will also contribute to the availability of water within the system, as well as potentially acting as a filler material that will not contribute to strength development if enough remains unreacted, as recorded in Nelson et al (2023) [17]. The relationship between w/s ratio and compressive strength development is demonstrated in the statistical analysis plot shown in Figure 11. Whilst an increase in water content does result in a decrease in the initial UPV value, correlating to the compressive strength results (Table 4), no relationship is seen with increasing gypsum content. There is also no relationship observed between mixing shear and developed product strength.

573

574

575

576

577

578

579

580581

582583

584

585

586

587588

589

590

591592

593

594595

The majority of strength development occurs within 7 d with the formation of ettringite, with a reduction in development rate as curing time progresses (Figure 10). This is also shown in the UPV values recorded. In some instances, a peak compressive strength is reached at 28 d, with a general slight reduction recorded at the \geq 90 d timepoint. However, one mix, outside the recommended formulation envelope at 35 wt.% gypsum incorporation and 0.5 w/s ratio did exhibit a significant strength loss from 50.1 MPa to 34 MPa between 28 d and 90 d. This behaviour is not consistent with any mix variable, and even considering the reduction in strength recorded, values are still consistent with other higher water mix results at equivalent gypsum contents and higher than the 2 d value. It is also notable in this particular mix that the 28 d strength far exceeds all other mixes with a gypsum content of > 15 % or w/s > 0.5 and could therefore be an outlier, with the compressive strength at 7 d and 90 d being 34.9 and 34.0 MPa respectively. The UPV data for this mix also does not suggest an increase in porosity as a cause for this decrease in compressive strength as values remain consistent. In Nelson et al (2023) [17], 35% gypsum content was shown to produce the highest ettringite content at 90 d of the formulation envelope tested, which could indicate that late stage ettringite growth is resulting in some internal stresses, though this is not demonstrated with any noticeable change in microstrain for this mix (Figure 9). Therefore, there is no variable presented in the phase assemblage [17], or in other experimental techniques such as the UPV or dimensional stability testing, that can account for this increase and later decrease in strength from this particular mix. The same formulation conducted with low shear also does not exhibit this behaviour. As compressive strength is a destructive testing method, it cannot be ruled out that this is specific to a particular set of samples tested on a certain date. Nevertheless, this particular formulation was not carried forward to later testing.

Table 4: Compressive strength data and UPV data generated from products of mixes at the 3 L scale. Values are averages taken from across three cubes.

Gypsum	CSA	w/s			UPV	(km/:	Compressive Strength (MPa)						
(wt.%) (wt.%) ratio		ratio	Shear			Ag	e (d)	Age (d)					
				2	7	28	56	70	≥ 90	2	7	28	≥ 90
15	85	0.5	Low	2.9	3.1	3.1	3.2	-	3.2 11	31.9	40.1	40.9	42.2
15	85	0.5	High	2.9	3.1	3.3	3.3	3.3	3.4	31.0	43.9	50.4	50.6
15	85	0.7	Low	2.5	2.6	2.7	-	-	2.7 11	22.8	25.6	25.3	29.5
15	85	0.7	High	2.5	2.7	2.7	-	-	2.8 11	23.2	27.3	31.5	30.5
25	75	0.6	Low	2.6	2.9	2.9	-	3.0	3.0	26.6	32.1	34.3	38.9
25	75	0.6	High	2.7	2.8	2.9	2.9	-	3.0	23.0	29.0	37.7	35.2
25	75	0.6	High	2.7	2.7	2.9	2.9	2.9	3.0	24.2	31.2	34.1	36.0
35	65	0.5	Low	2.8	2.9	3.1	-	3.1	3.2	25.5	32.5	37.9	43.1
35	65	0.5	High	2.8	3.0	3.2	3.2	-	3.3	26.7	34.9	50.1	34.0
35	65	0.7	Low	2.6	2.6	2.7	2.8	-	2.9 11	18.8	20.6	23.6	29.6
35	65	0.7	High	2.6	2.6	2.7	2.8	2.8	2.9	17.6	21.1	21.0	31.5



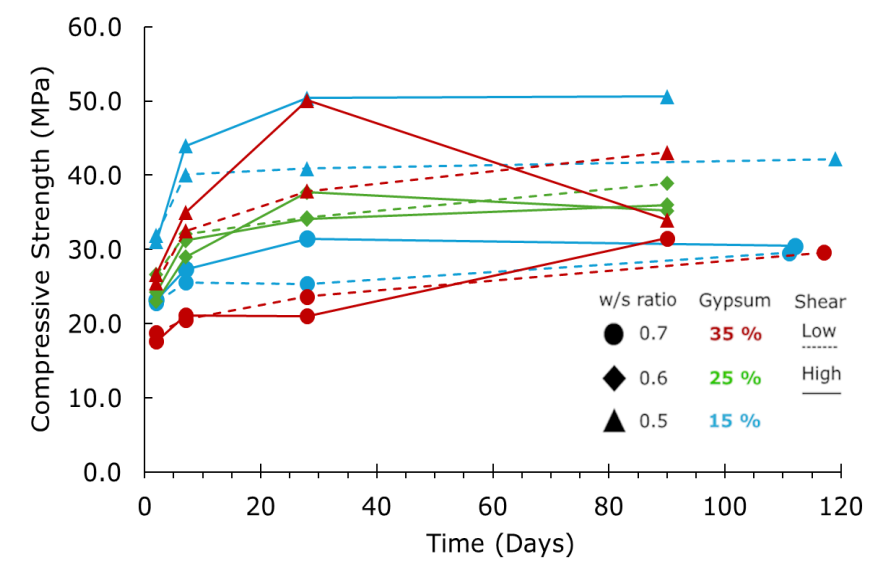


Figure 10: Compressive strength development with time, comparing the different mixing variables.

 $^{^{11}}$ Facility opening days, impacted by Covid-19, limited days that data could be collected. Curing ≥ 90 d was a duration of ~ 110 d.

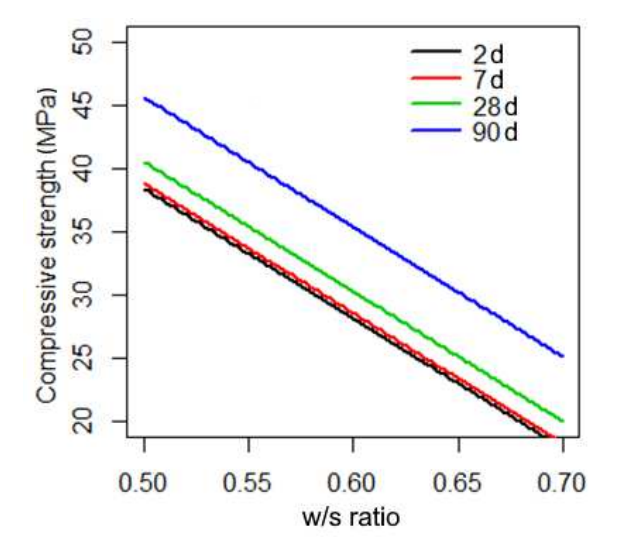


Figure 11: Statistical analysis of compressive strength development with w/s ratio, shown with different curing durations.

6. Results at the 500 L Scale

6.1. Identified Formulations

From the formulation envelope used in the 3 L scale mixes (Section 5), fluidity, setting, and heat of hydration properties aided the development of two mix designs, defined in Table 3, for assessment of the effect of high curing exotherms on product and microstructural properties at the 500 L scale. The influence of each property upon this development is discussed in their respective section. The defined formulations were produced to represent a higher (5G20, 20% gypsum w/s 0.65) and lower (5G35, 35% gypsum w/s 0.6) exotherm temperature mix design within the recommended formulation envelope.

6.2. Fluidity

In response to the results presented in Figure 4, the mix design for the subsequent two 500 L scale mixes feature a \geq 20 wt.% gypsum addition and a w/s ratio \geq 0.60 to retain a fluidity of > 500 mm Colflow throughout the full potential duration of a mix and hold-up. The w/s ratio was capped at 0.65 rather than 0.70 to reduce the inclusion of excess water in the mix, therefore reducing expected porosity and available water which may support metal corrosion reactions, whilst maintaining acceptable fluidity. Measurements taken from both 500 L scale mixes were both in agreement with Figure 4, with fluidities > 1020 mm at t=0. This suggests that the fluidity will remain > 500 mm Colflow at t=150.

6.3. Heat of Hydration

At the 3 L scale, the inclusion of gypsum at a level > 15 wt.% was shown to reduce the occurrence of an additional exotherm peak at between 8 - 16 h. Alongside the envelope

defined by the fluidity results (Sections 5.1 and 6.2), the decision to cap the w/s ratio at 0.65 was also aided by the increased heat of hydration with increasing water content (Figure 6).

Temperature profiles generated from the 500 L products (Figure 12) demonstrate that at this scale, product temperatures exceed 100 °C which will result in loss of water. These products were produced to test the limit of peak hydration exotherm and hence the thermal stability of ettringite in a theoretical neat cement product scenario with zero waste loading, a factor contributing significantly to the maximum product temperature achieved. Within each product, the most central point experiences the highest sustained temperature compared to the product extremities. Top and bottom sample temperatures were very similar; and are both represented closely by the minimum temperature curve.

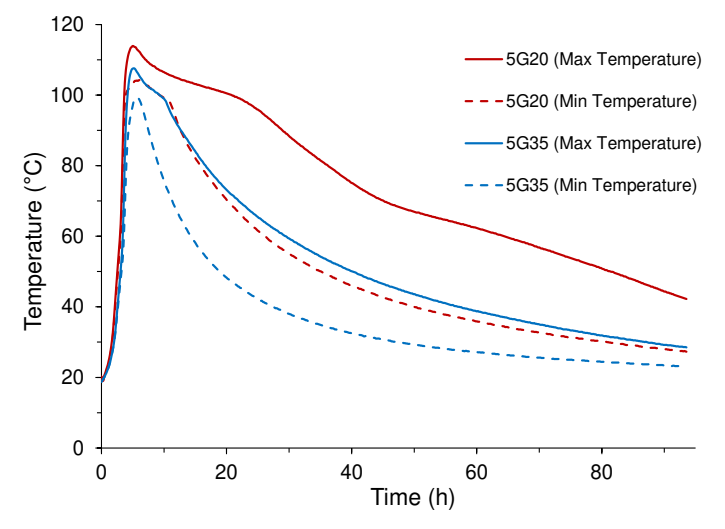


Figure 12: Temperature profile with time for 500 L products from mixes 5G20 and 5G35.

6.4. Setting Behaviour and Bleed

Lower availability of both water and gypsum was attributed to faster setting times at the 3 L scale (Figure 8). This again contributed to the selection of a higher water and gypsum content pair of formulations, albeit capped at 0.65 w/s as previously discussed. From samples taken from each 500 L mix, an initial set of between ≥ 2 and ≤ 3 h was recorded for mix 5G35, with the set of 5G20 exceeding operating hours, resulting in a recorded initial set span of ≥ 1 and ≤ 18 h. It is likely that an initial set would be achieved in a similar timeframe to 5G35, with little difference observed at similar formulations at the 3 L scale.

The result for 5G35 has therefore met the suggested ≥ 2 h initial set requirement, with the potential that 5G20 may have also achieved this timeframe. It is important to clarify that the setting time requirement is subject to an individual application, and therefore setting time alone may not rule out a formulation from future consideration. Final set of the 500 L product

was also achieved at between \geq 4.5 h and \leq 22 h (5G35), as well as \geq 1 h and \leq 18 h (5G20), meeting the < 48 h specification. Both mixes incorporated all the liquid component and generated no bleed.

659660661

662

663

664

665

666667

668

669670

671

657

658

- 6.5. Product Strength
- At the 500 L scale, the effect of the temperatures reached during hydration produced obvious structural weakness in the overall product, attributed to thermal stress, with cracks present in both products. The 5G20 product, which experienced the highest temperatures, was weakened to a considerable degree more than 5G35 and fell apart into large sections upon demoulding at 7 d curing (Figure 13). This necessitated 5G35 to be demoulded at 6 d curing to observe whether it could be sent for sectioning, for which it was deemed suitable (Figure 14). Compressive strength values differ little between 28 d and 90 d, in line with the expected rapid strength development of a CSA system. In this instance, UPV values could not be linked to strength development, likely due to the small changes in strength between 28 or 51, and 90 d, and therefore little change to the densification of products and the corresponding UPV values (Table 5).

672673

674

675

676

677

678679

680

681

682

683

684 685

686

687 688

689

690

691 692

693

Overall, 5G35 products have shown the greatest strength development, as would be expected given this 500 L product remained intact during demoulding. Products from 5G20 do not show any consistent behaviour based upon sample position, although both smaller cast samples did drop slightly in strength at 90 d. The 3 L mixes demonstrated that a reduced content of water, and to a lesser extent gypsum, both increased compressive strength development within that formulation envelope (Section 5.5). Despite 5G35 including a greater gypsum content, the lower w/s of 0.60 will reduce the availability of excess water, contributing towards greater compressive strength by producing a lower porosity matrix. The increased gypsum content also reduced the maximum exotherm temperature reached by reducing the overall ve'elimite content. Smaller cast cylinder products from 5G35 produced the highest compressive strength values encountered, likely due to the absence of introduced artefacts into the sample by the coring procedure as well as the exotherm temperature. The lowest compressive strength values originated from products taken from the central area of 5G20, which experienced the highest curing temperature. All results generated remain above the historically acceptable guidelines for product strength, however, the physical condition of 5G20 would not be considered acceptable. Direct comparison against strength values produced from 3 L products is difficult given the coring/cutting procedures used on samples produced from these 500 L mixes, which may introduce artefacts in the specimens accounting for the generally lower values achieved.

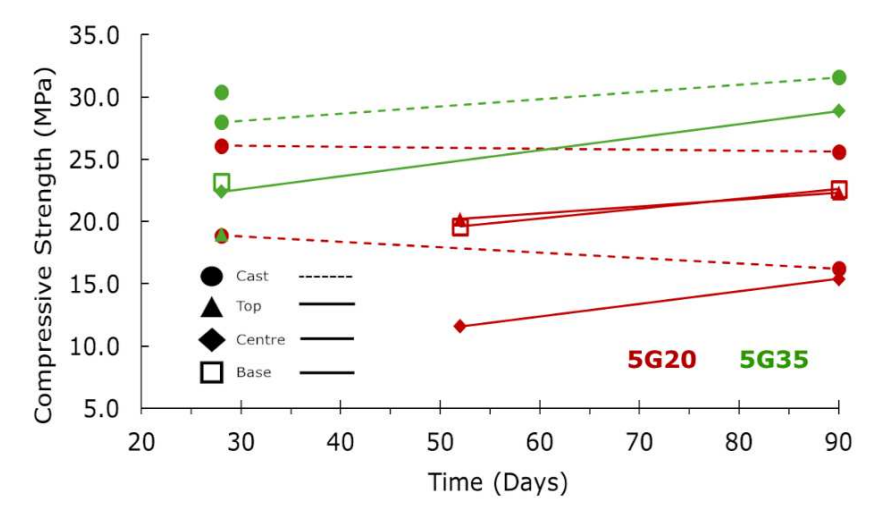


Figure 13: Demoulded 500 L product from mix 5G20 (left). Product broke up upon handling (right).



 $Figure \ 14: Demoulded \ 500 \ L \ product \ from \ mix \ 5G35 \ (left). \ Product \ interior \ surface \ after \ sectioning \ (right).$

Mix	Sample	CSA	Gypsum	w/s	UP	V (km	ı/s)	Compressive Strength (MPa)		
Reference	Location	(wt.%)	(wt.%)	ratio	A	ge (d)	12	Age (d) 12		
					28	51	90	28	51	90
	Small Cast Cylinder	80	20	0.65	2.9	-	2.9	26.1	-	25.6
5G20	Small Cast Cylinder	80	20	0.65	2.9	-	2.8	18.9	-	16.2
	Тор	80	20	0.65	-	2.7	2.7	-	20.2	22.3
	Centre	80	20	0.65	-	2.7	2.5	-	11.6	15.4
	Base	80	20	0.65	-	2.7	2.6	-	19.6	22.6
	Small Cast Cylinder	65	35	0.60	2.9	-	3.0	28.0	-	31.6
5G35	Small Cast Cylinder	65	35	0.60	3.0	-	-	30.4	-	_ 13
	Тор	65	35	0.60	2.6	-	-	19.0	-	-
	Centre	65	35	0.60	2.7	-	3.0	22.4	-	28.9
	Base	65	35	0.60	2.8	-	-	23.2	-	-



702 703

Figure 15: Compressive strength development with time for 500 L products. Sampling locations are denoted by symbols.

704705706

707

6.6. Phase Assemblage

6.6.1. X-ray diffraction and Rietveld Analysis

 $^{^{12}}$ Omitted values correspond to coring at 51 d as opposed to 28 d, or failed samples prior to testing.

 $^{^{13}}$ 5G35, one cylinder broke on demoulding and therefore, two 100 \times 100 mm cylinders were tested at 28 d and only one cylinder at 90 d.

In the XRD data acquired from 5G20 and 5G35 samples (Figure 16), high intensity diffraction peaks are observed for the reaction product ettringite (155395-ICSD) [54], as well as residual unreacted ye'elimite (80361-ICSD) [55], α -belite (orthorhombic) (81097-ICSD) [56], β -belite (monoclinic) (81096-ICSD) [56], and gypsum (230283-ICSD) [57]. Qualitative visual observation indicates that the diffraction patterns are nearly identical for all samples in both mixes at both 28 and 90 d after curing, with the one exception being the observation of greater quantities of ye'elimite in the smaller scale cast cylinder samples. Gołaszewska et al. (2021) [48] notes the effects of elevated curing temperatures significantly accelerating the hydration of CSA pastes, which may account for the greater utilisation of ye'elimite, differentiating the smaller cast samples from the higher temperature 500 L product samples.

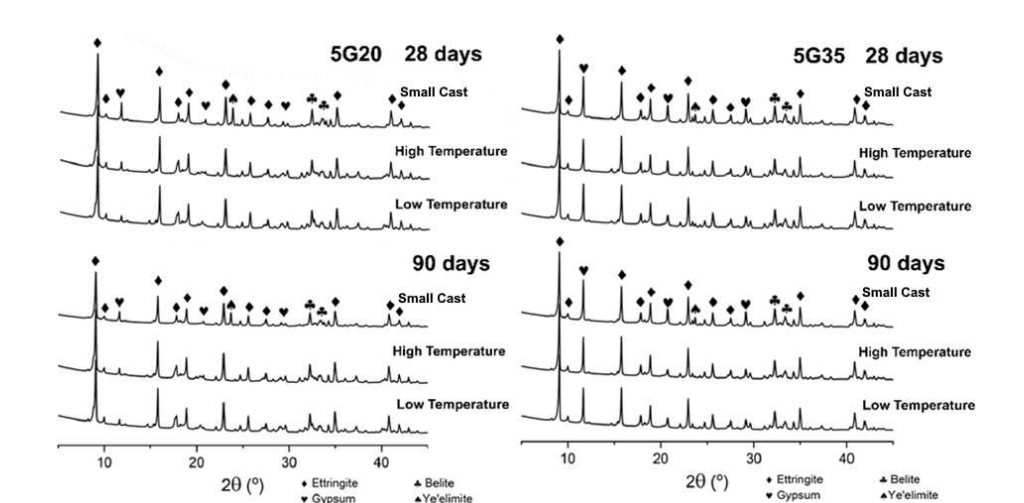


Figure 16: XRD data for the 5G20 (left) and 5G35 (right) mix at the 500L scale cured for 28 and 90 d, with small cast cylinder, high temperature, and lower temperature sourced samples shown as marked.

Quantification of the phase assemblage in these samples via Rietveld analysis identified a significant population of both ettringite and gibbsite, comparable with the phase assemblages of similar mixes identified in previous work [17], [39]. Within each mix, there is no discernible difference in the presence of ettringite, depending upon the exotherm temperature, at the curing time periods tested (Table 6). With some locations recording a temperature exceeding 100 °C, this suggests that ettringite reformed following the exposure to a temperature range wherein it may dehydrate or decompose; a potential given the availability of water and gypsum [25], [26], [32]. Levels of monosulfate, one of the expected main decomposition products of ettringite, also does not vary with increasing temperature (Figure 17).

Ettringite levels remain relatively constant with sample aging, with no suggestion of ettringite decomposition. Differences in ettringite content between 5G20 and 5G35 samples are likely therefore to be due to the increased availability of gypsum in 5G35 samples as shown in previous studies, and not related to temperature (Figure 18) [17], [39]. As shown in Figure 13,

internal stresses as a result of the high temperatures reached by the 5G20 500 L product have resulted in structural failure upon demoulding. These stresses could be purely thermal, causing crack propagation whilst the product structure is still in early development. The phase assemblage shows little difference between higher and lower temperature samples, however if ettringite were to reform having been exposed to high temperatures, its reformation could contribute towards internal stresses depending upon how it reforms [25], [26]. Described in Odler (2000) [4], oriented ettringite crystal growth, as opposed to a through-solution growth mechanism, could contribute to expansion not observed in experimentation at lower temperatures.

746 Table 6: Rietveld analysis from 500L mix products.

Mix & Sample	Days	Percentage Present (%)											
Reference	Days	Ettringite	Gibbsite	CSA	Gypsum	CSH	Monosulfate	C ₂ S	CH				
5G20	28	29	23	6	1	4	12	17	1				
(Max Temp)	90	29	22	7	2	4	12	18	1				
5G20	28	30	18	11	3	9	10	13	1				
(Min Temp)	90	30	23	10	2	4	12	13	1				
5G20	28	29	23	7	2	4	13	16	1				
(Small Cast)	90	30	23	7	2	4	13	15	1				
5G35	28	33	18	7	6	4	12	14	1				
(Max Temp)	90	37	17	7	6	4	11	11	1				
5G35	28	35	17	7	7	4	12	12	1				
(Min Temp)	90	35	20	7	6	4	11	11	1				
5G35	28	32	21	8	7	3	11	11	1				
(Small Cast)	90	32	21	8	7	4	11	11	1				

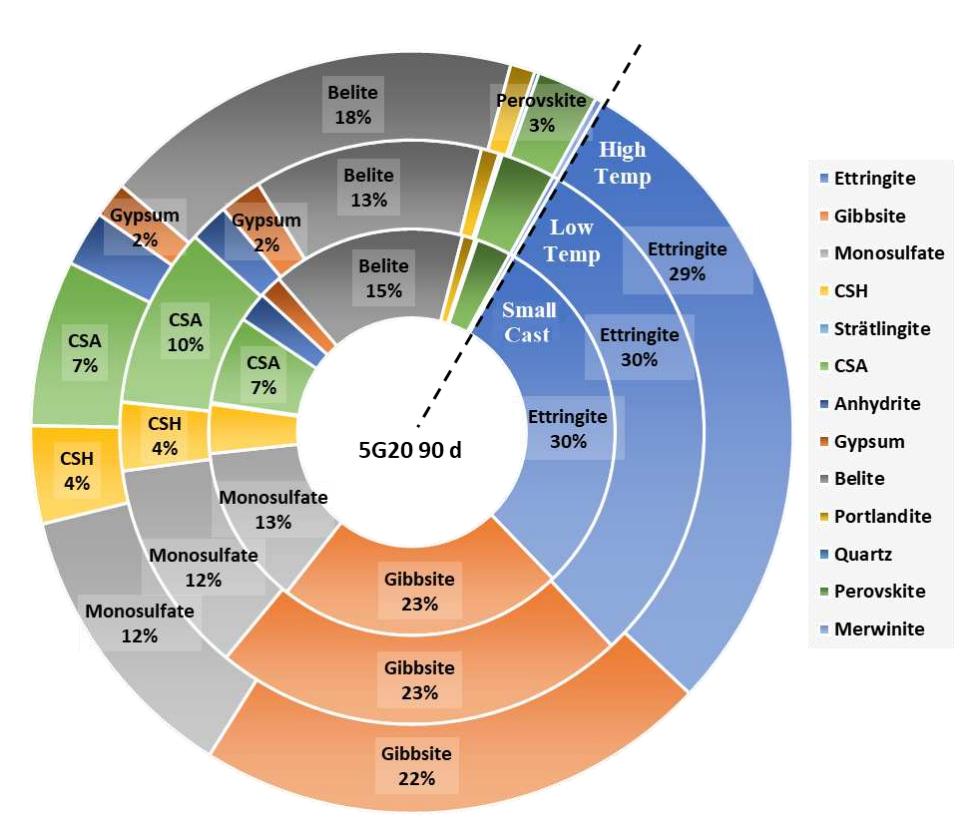


Figure 17: Phase assemblage plotted from Rietveld analysis of 5G20 at 90 d.

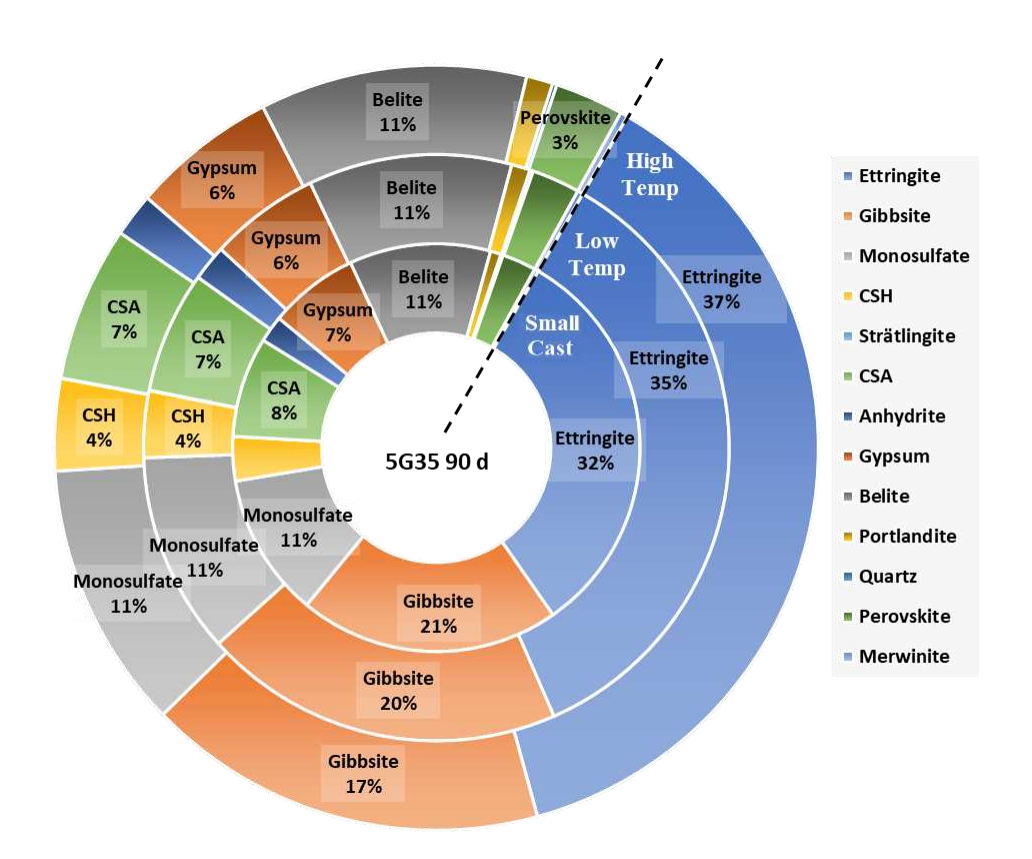


Figure 18: Phase assemblage plotted from Rietveld analysis of 5G35 at 90 d.

6.6.2. TGA

From TGA data obtained for all samples (Figure 19), four mass loss events were observed during heating, corresponding to; dehydroxylation of ettringite (100–120 °C), dehydroxylation of monosulfate and dehydration of residual unreacted gypsum (150 °C), dehydroxylation of gibbsite (240 °C), and thermal decomposition of calcium carbonate (650 °C). At each curing time, the mass loss and differential mass loss curves are very similar for all samples in both mixes.

The only discernible difference is seen in the data for the 5G20 mix cured for 28 d, for which the smaller cast cylinder sample exhibited a greater mass loss attributed the dehydration of residual unreacted gypsum, or potentially the dehydroxylation of monosulfate. An increased presence of either of these phases compared to 500 L product could indicate lower system reactivity, leading to a greater residual gypsum content with less being consumed in the production of ettringite, as well as increased monosulfate production. This does align with the trend observed for the XRD data discussed above, wherein the higher temperatures reached during the curing period increases the reactivity of the CSA paste, given that enough gypsum should be available in the system for the preferential generation of ettringite over monosulfate even at 20 % addition [48]. There is, however, little indication of increased gypsum or monosulfate presence within the XRD data, although this may be affected in part by the degree of monosulfate crystallinity [17], [39], [58].

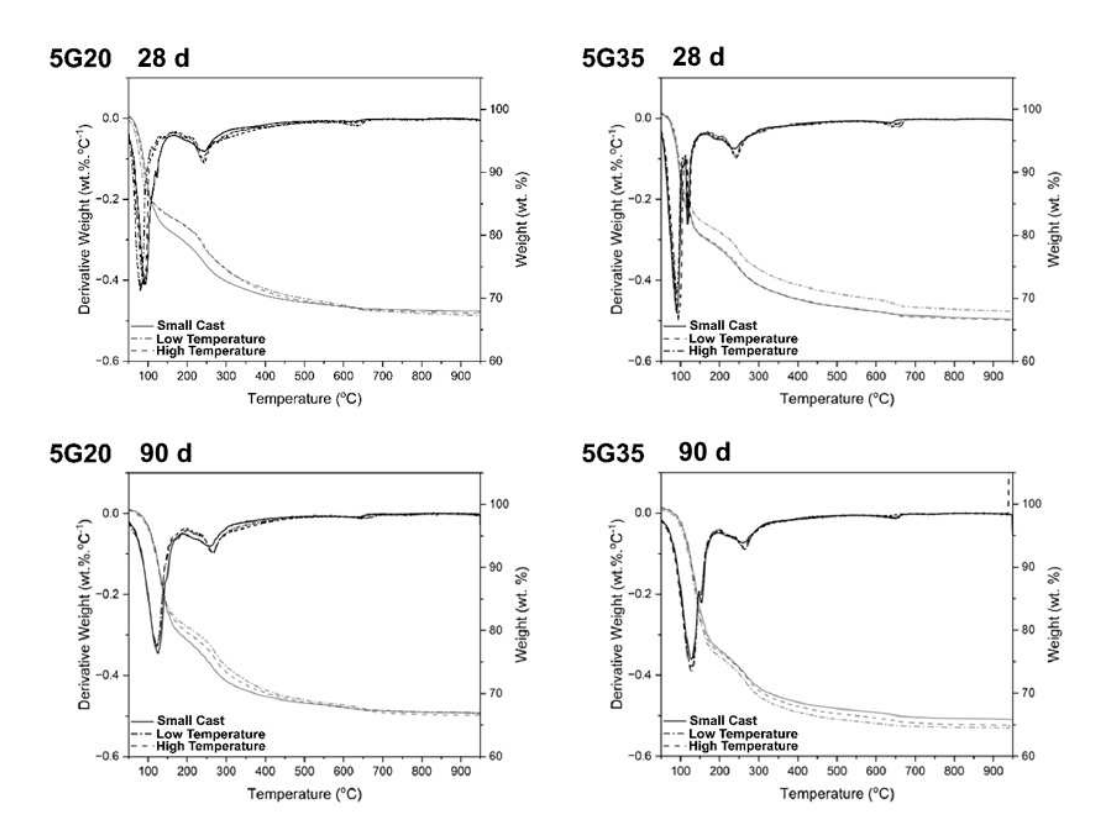


Figure 19: TGA data for the 5G20 and 5G35 mix at the 500L scale cured for 28 and 90 d, comparing small cast cylinder, low temperature, and high temperature sourced samples.

6.6.3. SEM-EDS

Backscattered electron (BSE) SEM images and EDS mapping data show the characteristic elemental signatures for ettringite and gibbsite, as well as residual unreacted ye'elimite, belite, and gypsum. The presence of ettringite, gibbsite (aluminium hydroxide), gypsum (calcium sulfate), and belite can be clearly identified in Figure 20 by the presence or absence of elemental signatures. Intense S concentration, with absence of Si and Al, and a large consistent particle size with dissolved edges shows partially/unreacted gypsum. The darker, amorphous surrounding phase that is high in Al but with lower levels of Ca, S and Si, depicts aluminium hydroxide. Ettringite is best identified by the noticeable crystal growth in the image, in areas with low Si content, with belite (or its hydrate phases) identifiable by the inclusion of significant Si content. Qualitative visual observation of these images shows no significant difference in the microstructure or phases assemblage at 90 d between samples obtained from the highest point of the 500 L exotherm, lowest, and those not exposed to it. This aligns with observations from the above XRD and TGA data, wherein the phase assemblage appears consistent between samples exposed to different temperature profiles. Similarly, the size and distribution of phases, particularly the ettringite, also appears to be relatively consistent.

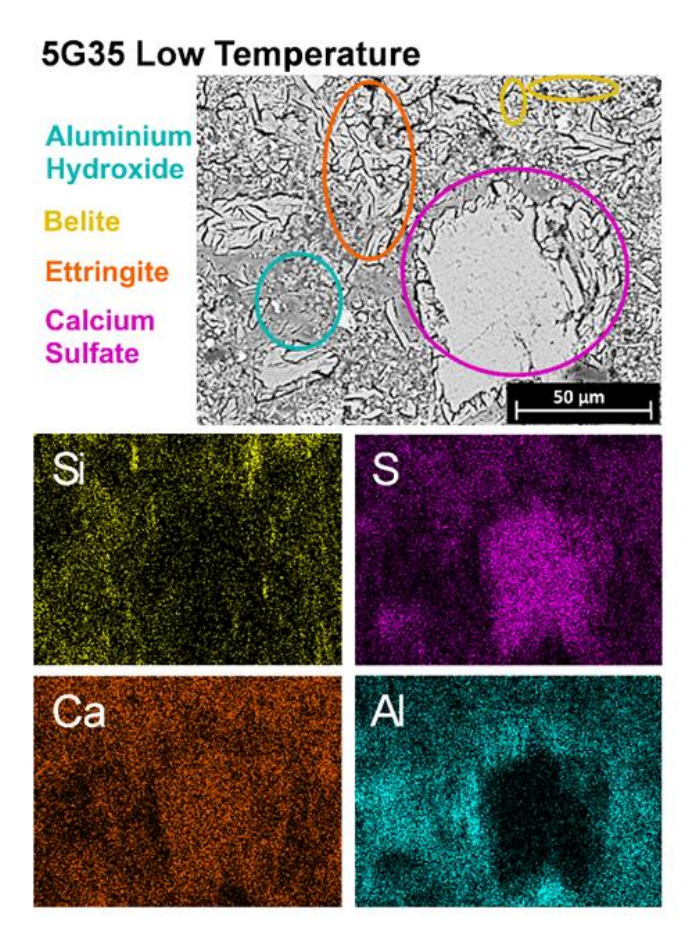


Figure 20: SEM-EDS image of a sample sourced from the low temperature region of the 5G35500 L product, and cured for 90 d, highlighting the visible phases that make up the majority of the phase assemblage.

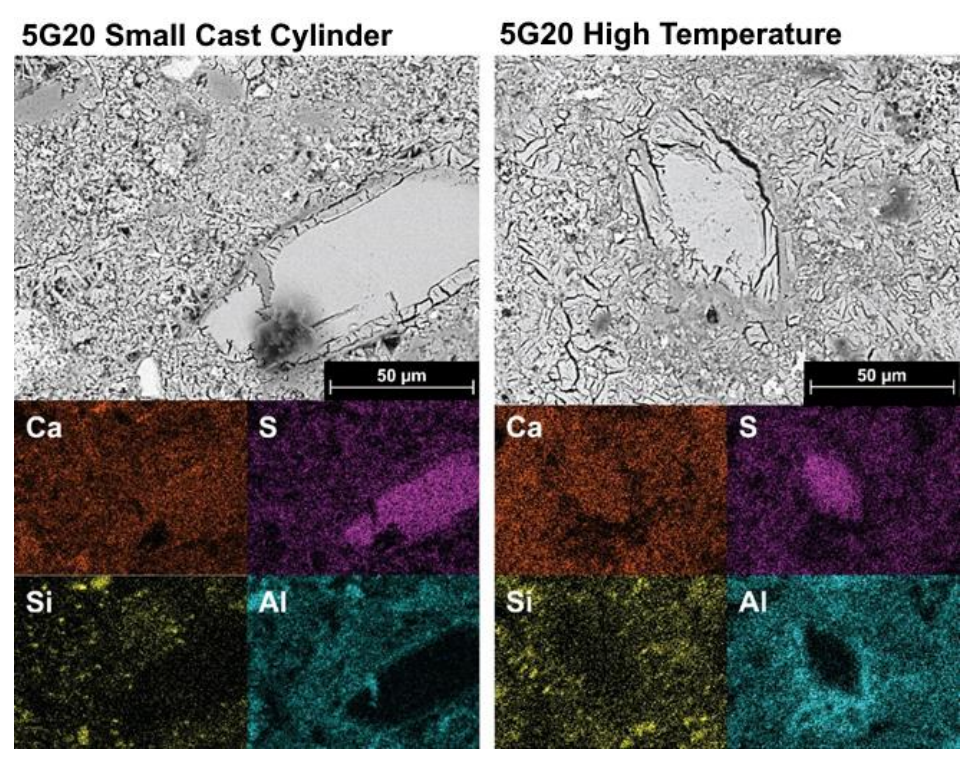


Figure 21: SEM-EDS images of 5G20 samples, cured for 90 d, sourced from the smaller cast cylinder sample (left) and the highest temperature region of the 500 L product (right).

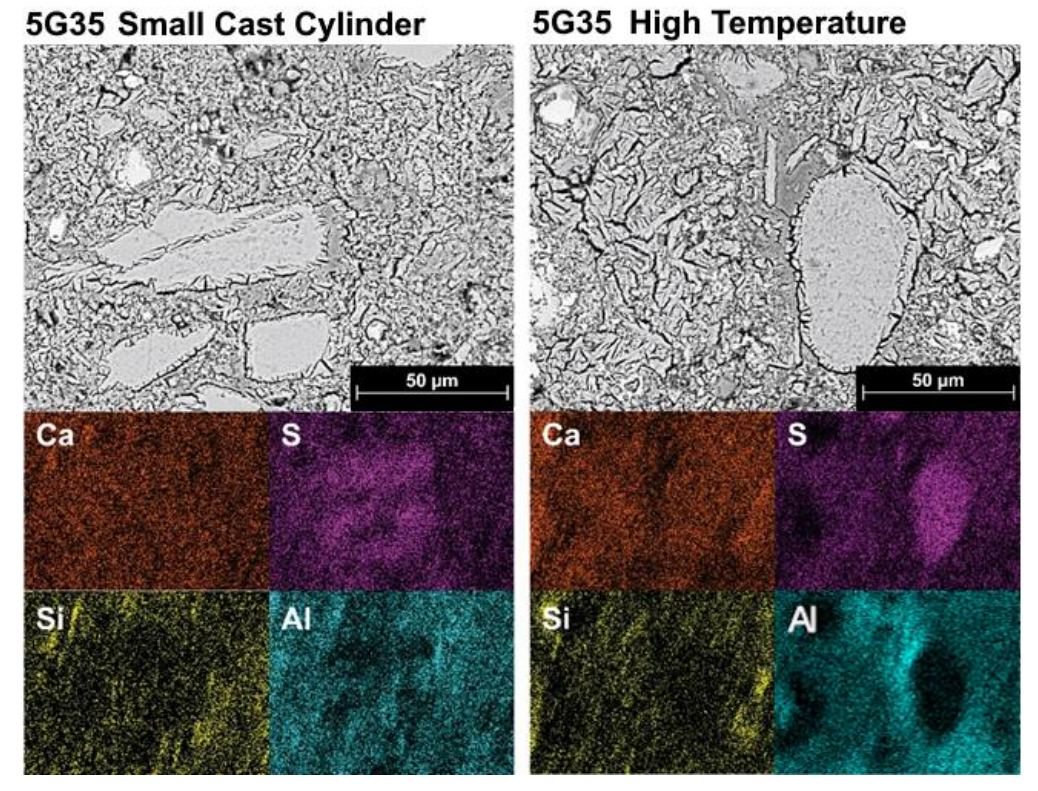


Figure 22: SEM-EDS images of 5G35 samples, cured for 90 d, sourced from the smaller cast cylinder sample (left) and the highest temperature region of the 500 L product (right).

7. Conclusions

Of the CSA formulations trialled, the mixes performed have demonstrated both desirable properties for all criteria, excluding that related to the generation of heat, as well as a consistent behaviour between 3 L and full 500 L scale trials representative of a typical IDM methodology.

Such properties include:

- The maintenance of fluidity for the total process duration (t=150) when w/s > 0.5.
- Initial and final sets achieved within a desirable timeframe.
- Acceptable mechanical strength results, decreasing with increased water content.
- The absence of any bleed.
- High dimensional stability.
- An increase in ettringite content with increasing gypsum content in the mix design.

The expected high temperature exotherms experienced by the neat, 500 L scale mix products, have demonstrated that whilst affecting product integrity, it has not noticeably impacted upon the phase assemblage produced following the 28 d minimum curing period. This is despite both 500 L products exceeding 100 °C in some areas, with no significant difference in ettringite content observed between regions. This suggests a degree of ettringite rehydration

as well as reformation if ettringite has dehydrated under these conditions, given the availability of the necessary water as well as calcium sulfate. It also suggests that ionic species retention may persist under these conditions. Increased system temperature has also shown greater consumption of ye'elimite and gypsum. Cumulative heat of hydration was increased with the greater availability of water and reduced with the greater fraction of gypsum present. Mixing shear did not impact upon the cumulative heat of hydration after 24 h, but did increase the initial exotherm peak of the normalised heat flow. A gypsum content of > 15 % and < 35 % produced an additional exotherm peak, which is delayed and reduced with increasing gypsum content.

Whilst the maximum temperature experienced by the 500 L products is not representative of a wasteform that will include a significant proportion of waste material, or an encapsulation grout containing predominantly SCM as currently employed, future study into the behaviour of CSA subjected to temperatures in excess of the stability of ettringite would be advantageous. This could be conducted with reference to interim and expected long-term storage environments, such as when part of an EBS within a GDF. Monitoring the early stage hydration of CSA and phase development, under the influence of high curing temperatures and other curing conditions, would allow for the mechanism behind whether ettringite is reformed or rehydrated to be deciphered. Furthermore, the study of the interactions between CSA and a chosen waste material, as well as any potential SCM, is required to enable future development and deployment.

8. Acknowledgements

Shaun Nelson: Methodology, Investigation, Formal analysis, Data curation, Writing – original draft, Visualisation. Sally Cockburn: Methodology, Investigation, Formal analysis, Data curation, Writing – review & editing, Visualisation. Olivia Tuck: Formal analysis, Data curation, Visualisation. Martin Hayes: Conceptualisation, Methodology, Writing – review & editing. Gavin Cann: Conceptualisation, Methodology, Writing – review & editing. Cameron Halliwell: Data curation, Investigation, Formal analysis, Visualisation. Daniel Geddes: Data curation, Investigation, Formal analysis, Visualisation. Brant Walkley: , Investigation, Formal analysis, Writing – original draft, review & editing, Visualisation. Stephen Farris: Conceptualisation, Methodology, Writing – review & editing.

Funding for this work was provided by Sellafield Ltd.

9. References

881 882

883

884

887 888

889 890 891

892

893

894

895

896

- 856 [1] Q. Zhou, N. B. Milestone, and M. Hayes, 'An alternative to Portland Cement for waste encapsulation—The calcium sulfoaluminate cement system', *Journal of Hazardous Materials*, vol. 136, no. 1, pp. 120–129, Aug. 2006, doi: 10.1016/j.jhazmat.2005.11.038.
- 859 [2] F. Bertola, D. Gastaldi, S. Irico, G. Paul, and F. Canonico, 'Influence of the amount of calcium sulfate on physical/mineralogical properties and carbonation resistance of CSA-based cements',
 861 **Cement and Concrete Research*, vol. 151, 2022, doi:
 862 **https://doi.org/10.1016/j.cemconres.2021.106634.*
- [3] E. Bescher and J. Kim, 'Belitic calcium sulfoaluminate cement: history, chemistry, performance, and use in the United States', in *Proceedings of the 1st International Conference on Innovation in Low-Carbon Cement and Concrete Technology*, University College London, 2019.
- 866 [4] 'Expansive Cements', in *Special Inorganic Cements*, 1st ed., in Modern Concrete Technology 867 Series. , London, UK: CRC Press, 2000, pp. 297–316. [Online]. Available: https://doi.org/10.1201/9781482271942
- 869 [5] S. Galluccio, T. Beirau, and H. Pöllmann, 'Maximization of the reuse of industrial residues for the 870 production of eco-friendly CSA-belite clinker', *Construction and Building Materials*, vol. 208, pp. 871 250–257, May 2019, doi: 10.1016/j.conbuildmat.2019.02.148.
- 872 [6] M. García-Maté, 'Processing and characterisation of calcium sulphoaluminate (CSA) eco-cements with tailored performances', Universidad de Malaga, Spain, 2014.
- P. C. Hewlett and M. Liska, Eds., 'The production of low energy cements', in *Lea's Chemistry of Cement and Concrete*, Fifth Edition., 2019, pp. 341–362.
- 876 [8] S. Kearney, 'Radiolysis and radiation damage effects in cements used in nuclear waste storage and disposal in the UK', The University of Sheffield, UK, 2020.
- 878 [9] S. Kearney *et al.*, 'Cement-based stabilization/solidification of radioactive waste', in *Low Carbon Stabilization and Solidification of Hazardous Wastes*, 1st ed., D. C. W. Tsang and L. Wang, Eds., Elsevier, 2022, pp. 407–431. doi: 10.1016/B978-0-12-824004-5.00005-0.
 - [10] M. J. Angus, I. H. Godfrey, M. Hayes, and S. Foster, 'Managing Change in the Supply of Cement Powders for Radioactive Waste Encapsulation Twenty Years of Operational Experience', in Session 31 Operating Experience in the Treatment and Storage of LLW, ILW, and TRU, Phoenix, Arizona, US: National Nuclear Laboratory, 2010.
- [11] M. I. Ojovan and W. E. Lee, 'Immobilisation of Radioactive Wastes in Cement', in *An Introduction to Nuclear Waste Immobilisation*, 2nd ed., Elsevier, 2014, pp. 205–232.
 - [12]F. P. Glasser and R. Spence, 'Chemistry of Cement-Solidified Waste Forms', in *Chemistry and microstructure of solidified waste forms*, 1992. [Online]. Available: https://openlibrary.org/works/OL21219471W/Chemistry_and_Microstructure_of_Solidified_Waste_Forms
 - [13] A. Atteridge and C. Strambo, 'Decline of the United Kingdom's steel industry: lessons from industrial transitions', Stockholm Environment Institute, 2021. [Online]. Available: DOI: 10.51414/sei2021.013
 - [14] M. J. Angus, J. Borwick, G. Cann, M. Hayes, B. H. McLuckie, and J. Jowsey, 'The Specification of Cement Powders for Waste Encapsulation Processes at Sellafield site', presented at the International Symposium on Cement-Based Materials for Nuclear Wastes, Avignon, France, 2011, pp. 48–58.
- 898 [15]E. Gartner, 'Industrially interesting approaches to "low-CO₂" cements', *Cement and Concrete Research*, vol. 34, no. 9, pp. 1489–1498, Sep. 2004.
- [16] C. W. Hargis, A. P. Kirchheim, P. J. M. Monteiro, and E. M. Gartner, 'Early age hydration of calcium sulfoaluminate (synthetic ye'elimite, C4A3S) in the presence of gypsum and varying amounts of calcium hydroxide', *Cement and Concrete Research*, vol. 48, pp. 105–115, Jun. 2013, doi: 10.1016/j.cemconres.2013.03.001.
- 904 [17]S. Nelson *et al.*, 'Hydrate assemblage stability of calcium sulfoaluminate-belite cements with varying sulfate content', *Construction and Building Materials*, vol. 383, Jun. 2023, doi: 10.1016/j.conbuildmat.2023.131358.

- 907 [18]I. Bolaños-Vásquez, R. Trauchessec, J. I. Tobón, and A. Lecomte, 'Influence of the ye'elimite/anhydrite ratio on PC-CSA hybrid cements', *Materials Today Communications*, vol. 22, Mar. 2020, doi: 10.1016/j.mtcomm.2019.100778.
- 910 [19]M. L. D. Gougar, B. E. Scheetz, and D. M. Roy, 'Ettringite and C-S-H Portland cement phases for waste ion immobilization: A review', *Waste Management*, vol. 16, no. 4, pp. 295–303, Jan. 1996, doi: 10.1016/S0956-053X(96)00072-4.
- [20]S. A. Saslow *et al.*, 'Immobilizing Pertechnetate in Ettringite via Sulfate Substitution', *Environ. Sci. Technol.*, vol. 54, no. 21, pp. 13610–13618, Nov. 2020, doi: 10.1021/acs.est.0c03119.

- [21] A. Jiménez and M. Prieto, 'Thermal Stability of Ettringite Exposed to Atmosphere: Implications for the Uptake of Harmful Ions by Cement', *Environ. Sci. Technol.*, vol. 49, no. 13, pp. 7957–7964, Jul. 2015, doi: 10.1021/acs.est.5b00536.
- 918 [22]Y. V. Seryotkin, E. V. Sokol, S. N. Kokh, and M. N. Murashko, 'Natural Cr3+-rich ettringite: occurrence, properties, and crystal structure', *Physics and Chemistry of Minerals*, vol. 45, no. 3, pp. 279–292, Mar. 2018, doi: 10.1007/s00269-017-0917-y.
 - [23] A. S. Yorkshire *et al.*, 'Spectroscopic identification of Ca-bearing uranyl silicates formed in C–S–H systems', *Scientific Reports*, vol. 13, no. 1, p. 3374, Feb. 2023, doi: 10.1038/s41598-023-30024-0.
 - [24] Q. Zhou, E. E. Lachowski, and F. P. Glasser, 'Metaettringite, a decomposition product of ettringite', *Cement and Concrete Research*, vol. 34, no. 4, pp. 703–710, Apr. 2004, doi: 10.1016/j.cemconres.2003.10.027.
 - [25]Q. Zhou and F. P. Glasser, 'Thermal stability and decomposition mechanisms of ettringite at <120°C', *Cement and Concrete Research*, vol. 31, no. 9, pp. 1333–1339, Sep. 2001, doi: 10.1016/S0008-8846(01)00558-0.
 - [26] L. G. Baquerizo, T. Matschei, and K. L. Scrivener, 'Impact of water activity on the stability of ettringite', *Cement and Concrete Research*, vol. 79, pp. 31–44, Jan. 2016, doi: 10.1016/j.cemconres.2015.07.008.
 - [27]K. Ndiaye, M. Cyr, and S. Ginestet, 'Durability and stability of an ettringite-based material for thermal energy storage at low temperature', *Cement and Concrete Research*, vol. 99, pp. 106–115, Sep. 2017, doi: 10.1016/j.cemconres.2017.05.001.
 - [28]T. Honorio, 'Multi-Scale Multi-Physics Multi-Technique modeling for establishing composition-(micro)structure-property correlations in cement-based materials. HDR (Habilitation à Diriger des Recherches).', University of Paris-Saclay, 2023. doi: 10.13140/RG.2.2.22787.58403.
 - [29]S. Yamaguchi and T. Hongo, 'Synthesis of metaettringite from blast furnace slag and evaluation of its boron adsorption ability', *Environmental Science and Pollution Research*, vol. 28, no. 12, pp. 15070–15075, Mar. 2021, doi: 10.1007/s11356-020-11028-z.
 - [30] A. Iizuka, M. Takahashi, T. Nakamura, and A. Yamasaki, 'Preparation of Metaettringite from Ettringite and Its Performance for Boron Removal from Boric Acid Solution', *MATERIALS TRANSACTIONS*, vol. 58, no. 12, pp. 1761–1767, 2017, doi: 10.2320/matertrans.M-M2017839.
 - [31] A. Iizuka, H.-J. Ho, and A. Yamasaki, 'Removal of fluoride ions from aqueous solution by metaettringite', *PLOS One*, vol. 17, p. 18, Mar. 2022, doi: 10.1371/journal.pone.0265451.
 - [32] J. Kaufmann, F. Winnefeld, and B. Lothenbach, 'Stability of ettringite in CSA cement at elevated temperatures', *Advances in Cement Research*, vol. 28, no. 4, pp. 251–261, 2016, doi: 10.1680/jadcr.15.00029.
 - [33]H. F. W. Taylor, C. Famy, and K. L. Scrivener, 'Delayed ettringite formation', *Cement and Concrete Research*, vol. 31, no. 5, pp. 683–693, May 2001, doi: 10.1016/S0008-8846(01)00466-5.
- [34]Q. Liu *et al.*, 'Quantifying the immobilization mechanisms of heavy metals by Calcium Silicate Hydrate (C-S-H): The case of Cu2+', *Cement and Concrete Research*, vol. 186, 2024, doi: 10.1016/j.cemconres.2024.107695.
- 955 [35]E. Duque-Redondo, K. Yamada, and H. Manzano, 'Effect of Chloride and Sulfate in the Immobilization of Cs-137 in C-S-H Gel', *Journal of Advanced Concrete Technology*, vol. 19, no. 1, pp. 95–105, 2021, doi: 10.3151/jact.19.95.
- [36]M. Isaacs *et al.*, 'Processing and product characteristics of a blended cement grout incorporating polycarboxylate ether superplasticiser', *Advances in Cement Research*, vol. 30, pp. 1–11, 2018, doi: 10.1680/jadcr.17.00102.

- [37] Radioactive Waste Management Ltd, 'Waste Package Specification and Guidance Documentation:
 Specification for Waste Packages Containing Low Heat Generating Waste: Part C Fundamental
 Requirements', Nuclear Decomissioning Authority, WPS/220/01, 2020. [Online]. Available:
 https://assets.publishing.service.gov.uk/media/5fb297df8fa8f55de86fb394/WPS_220_01_Part_C_
 Specification for Waste Packages Containing Low Heat Generating Waste.pdf
- [38] J. Ambrose, V. K. Shenbagam, J. L. Provis, É. P. Bescher, and T. Hanein, 'Assessment of standard test procedures applied to calcium sulfoaluminate based cements', *Advances in Cement Research*, vol. 37, no. 2, pp. 125–132, 2025, doi: 10.1680/jadcr.24.00033.
- 969 [39]S. Nelson, 'Cements of the Future and Future Nuclear Cements', The University of Sheffield, UK, 970 2023.

- [40] British Standards Institution, BS EN 1097-7:2008; Tests for mechanical and physical properties of aggregates Part 7: Determination of the particle density of filler Pyknometer method, BS EN 1097-7:2008, 2008.
- [41] C. Katsari, Y. Kotsakis, S. Yue, B. Guerreiro, D. Poirier, and J. Giallonardo, 'Oxide characterization of copper cold spray feedstock powders with X-Ray Photoelectron Spectroscopy', in *Proceedings from the International Thermal Spray Conference*, Quebec, Canada: ASM International, 2023, pp. 91–97. doi: https://doi.org/10.31399/asm.cp.itsc2023p0091.
- [42] British Standards Institution, BS EN 13395-2:2002 Products and systems for the protection and repair of concrete structures Test methods Determination of workability Part 2: Test for flow of grout or mortar, BS EN 13395-2:2002, 2002.
- [43] British Standards Institution, BS EN 196-3:2005+A1:2008 Methods of testing cement Part 3: Determination of setting times and soundness, BS EN 196-3:2005+A1:2008, 2008.
- [44] American Society for Testing and Materials, ASTM C490; Standard Practice for use of Apparatus for the Determination of Length Change of Hardened Cement Paste, Mortar, and Concrete, C490/C490M 21, 2021.
- [45]K. Scrivener, R. Snellings, and B. Lothenbach, A Practical Guide to Microstructural Analysis of Cementitious Materials, 1st ed. CRC Press, 2018.
- [46] The R Core Team, R: A Language and Environment for Statistical Computing, Version 4.5.1. 2025. [Online]. Available: https://www.r-project.org/
- [47]L. Zhang, M. Su, and Y. Wang, 'Development of the use of sulfo- and ferroaluminate cements in China', *Advances in Cement Research*, vol. 11, no. 1, pp. 15–21, 1999, doi: 10.1680/adcr.1999.11.1.15.
- [48] M. Gołaszewska, B. Klemczak, and J. Gołaszewski, 'Thermal Properties of Calcium Sulphoaluminate Cement as an Alternative to Ordinary Portland Cement', *Materials*, vol. 14, no. 22, 2021, doi: 10.3390/ma14227011.
 - [49] C. Cau Dit Coumes, O. Farcy, P. Antonucci, J.-B. Champenois, D. Lambertin, and A. Mesbah, 'Design of self-desiccating binders using CSA cement: influence of the cement composition and sulfate source', *Advances in Cement Research*, vol. 31, no. 4, pp. 178–194, 2019, doi: 10.1680/jadcr.18.00100.
- [50]F. Winnefeld and S. Barlag, 'Calorimetric and thermogravimetric study on the influence of calcium sulfate on the hydration of ye'elimite', *Journal of Thermal Analysis and Calorimetry*, vol. 101, no. 3, pp. 949–957, Sep. 2010, doi: 10.1007/s10973-009-0582-6.
- 1003 [51]S. Goto and D. M. Roy, 'The effect of w/c ratio and curing temperature on the permeability of hardened cement paste', *Cement and Concrete Research*, vol. 11, no. 4, pp. 575–579, Jul. 1981, doi: 10.1016/0008-8846(81)90087-9.
- [52]H. F. W. Taylor, 'Structure and properties of fresh and hardened Portland cement pastes', in *Cement Chemistry*, 2nd ed., London: Thomas Telford, 1997, pp. 227–260.
- 1008 [53]Y.-Y. Kim, K.-M. Lee, J.-W. Bang, and S.-J. Kwon, 'Effect of W/C Ratio on Durability and Porosity in Cement Mortar with Constant Cement Amount', *Advances in Materials Science and Engineering*, p. Rietveld crystal structure refinements, crystal chemistry a, 2024, doi: 10.1155/2014/273460.
- 1012 [54]F. Goetz-Neunhoeffer and J. Neubauer, 'Refined ettringite (Ca6Al2(SO4)3(OH)12·26H2O) structure for quantitative X-ray diffraction analysis', *Powder Diffraction*, vol. 21, no. 1, pp. 4–11, 2006, doi: 10.1154/1.2146207.

- 1015 [55]N. J. Calos, C. H. L. Kennard, A. K. Whittaker, and R. L. Davis, 'Structure of calcium aluminate sulfate Ca4Al6O16S', *Journal of Solid State Chemistry*, vol. 119, no. 1, pp. 1–7, Oct. 1995, doi: 10.1016/0022-4596(95)80002-7.
- 1018 [56] W. G. Mumme, R. J. Hill, G. Bushnell-wye, and E. R. Segnit, 'Rietveld crystal structure refinements, crystal chemistry and calculated powder diffraction data for the polymorphs of dicalcium silicate and related phases', *New Yearbook of Mineralogy Papers*, vol. 170, no. 2, 1996, [Online]. Available: https://api.semanticscholar.org/CorpusID:135973945
- 1022 [57]T. Fukami, S. Tahara, K. Nakasone, and C. Yasuda, 'Synthesis, Crystal Structure, and Thermal 1023 Properties of CaSO4·2H2O Single Crystals', *International Journal of Chemistry*, vol. 7, no. 2, 2015, doi: 10.5539/ijc.v7n2p12.
- 1025 [58]D. Gastaldi *et al.*, 'Hydration products in sulfoaluminate cements: Evaluation of amorphous phases by XRD/solid-state NMR', *Cement and Concrete Research*, vol. 90, pp. 162–173, Dec. 2016, doi: 10.1016/j.cemconres.2016.05.014.